

## Predictable and Unpredictable Aspects of U.S. West Coast Rainfall and El Niño: Understanding the 2015/16 Event

BENJAMIN A. CASH AND NATALIE J. BURLS

*Center for Ocean–Land–Atmosphere Studies, George Mason University, Fairfax, Virginia*

(Manuscript received 26 March 2018, in final form 1 December 2019)

### ABSTRACT

California experienced record-setting drought from 2012 to 2017. Based on both seasonal forecast models and historical associations, there was widespread expectation that the major El Niño event of 2015/16 would result in increased winter-season precipitation and break the drought. However, the 2015/16 winter rainy season ultimately resulted in slightly below-average precipitation and the drought continued. In this work we analyze data from both observations and seasonal forecasts made as part of the North American Multi-Model Ensemble (NMME) to better understand the general relationship between El Niño and U.S. West Coast rainfall, focusing on Southern California (SOCAL) rainfall, Pacific Northwest (PNW) rainfall, and the 2015/16 event. We find that while there is a statistically significant positive correlation between El Niño events and the SOCAL and PNW rainfall anomalies, this relationship explains at most one-third of the observed variance. Examination of hindcasts from the NMME demonstrates that the models are capable of accurately reproducing this observed correlation between tropical Pacific sea surface temperatures and California rainfall when information from the individual ensemble members is retained. However, focusing on the multimodel ensemble mean, which deliberately reduces the influence of unpredicted variability, drastically overestimates the strength of this relationship. Our analysis demonstrates that much of the winter rainfall variability along the U.S. West Coast is dominated by unpredicted variations in the 200-hPa height field and that this same unpredicted variability was largely responsible for the unexpectedly dry conditions in 2015/16.

### 1. Introduction


The California drought of 2012–17 was exceptionally severe. At its peak the entire state experienced drought conditions and over 40% of the state was in the most severe category (D4; U.S. Drought Monitor), and less severe drought conditions were present across the entirety of Washington and Oregon as well. Drought conditions arose due to persistent precipitation deficits during the key boreal winter wet season that were among the most intense recorded (e.g., Hoell et al. 2016).

In early 2015, a high-amplitude El Niño event developed and persisted through the winter of 2015/16. Based on historical associations (see Hoell et al. 2016, and references therein), it was widely anticipated that this event would bring above-average precipitation to

Southern California (SOCAL) and alleviate the drought there. This historical inference was reinforced by predictions from multiple seasonal forecast models (see section 3 for further discussion). However, rainfall remained below normal throughout the winter, and the drought continued in SOCAL until the record-breaking rainfall of winter 2016/17 led to the official end of the drought in early 2017. In contrast, the Pacific Northwest (PNW) received equally unpredicted above-normal rainfall, which brought an end to drought conditions in that region.

The failure of the seasonal rain predictions in the winter of 2015/16, along with the subsequent and equally unpredicted end to the California drought in the winter of 2016/17, has raised questions about the predictability of California seasonal rainfall in particular, as well as its general relationship with El Niño–Southern Oscillation (ENSO). California is known to be influenced by several midlatitude responses to ENSO, namely the Pacific–North America (PNA) pattern, the strengthened Aleutian low, an enhanced southward-shifted subtropical jet, and

---

 Denotes content that is immediately available upon publication as open access.

---

*Corresponding author:* Benjamin A. Cash, bcash@gmu.edu

increased tropical storms in the eastern Pacific generally leading to enhanced winter precipitation during El Niño events (e.g., [Schonher and Nicholson 1989](#); [Seager et al. 2010](#); [Trenberth et al. 1998](#)). The association with ENSO is the opposite for the PNW with precipitation generally reduced during El Niño events and enhanced during La Niña events ([Mo and Higgins 1998](#); [Dettinger et al. 1998](#); [Yu and Zou 2013](#)), although the strength of the association between ENSO and precipitation variability is stronger for SOCAL, and as a result the majority of studies focus on the latter region.

[Schonher and Nicholson \(1989\)](#) present one of the first studies suggesting that 1) the response of California rainfall to El Niño depends on the nature of the SST warming pattern (El Niño type and duration) and 2) that the response of California rainfall to an El Niño event is regionally specific, with the greatest tendency for enhanced rainfall over Southern California. According to a number of studies, strong positive SST anomalies in the eastern equatorial Pacific that persist late into the winter appear to have the strongest association with enhanced Southern California rainfall ([Schonher and Nicholson 1989](#); [Jong et al. 2016](#); [Lee et al. 2017](#)).

In contrast to the studies listed above, [Yu and Zou \(2013\)](#) use reanalysis data and atmospheric general circulation experiments to suggest that the “wetting effect” of El Niño events in Southern California is stronger in response to a central Pacific El Niño warming pattern, rather than the canonical eastern Pacific warming pattern. The authors found that central Pacific warming results in the tropospheric jet streams being displaced farther to the south, thus steering moisture into Southern California. However, over Northern California, the PNW and other regions within the United States, central Pacific El Niño events typically result in drier conditions than eastern Pacific events. [Kim et al. \(2017\)](#) also find that for central Pacific El Niño events the Aleutian low shifts farther south, increasing the occurrence and intensity of atmospheric rivers over the southwestern United States relative to eastern Pacific El Niño events.

[Jong et al. \(2016\)](#) suggest that El Niño’s influence on California is strongest in the south due to the increasing influence of midlatitude systems farther north and highlight the asymmetry in the impact of ENSO. They find that when only El Niño events are considered the correlation coefficients in Northern and Southern California are similar for late winter rainfall anomalies. The authors suggest that this feature may be due to asymmetries in the teleconnection patterns for El Niño and La Niña events (see [Hoerling et al. 1997](#)).

When evaluating the potential effect of El Niño events, it is important to recognize the unique aspects of California rainfall relative to other regions within the

United States. Most notably, California receives most of its annual precipitation over only a few days each year. As a result, it experiences particularly large interannual rainfall variability (see [Myoung and Deng 2009](#); [Dettinger et al. 2011](#)). The difference between a high rainfall year and a drought is typically determined by the presence or absence of a few large storms that are generally associated with atmospheric rivers. While some studies suggest that the frequency of atmospheric river events along the west coast of North America increases during El Niño years relative to La Niña years ([Guan and Waliser 2015](#); [Kim et al. 2017](#)), analysis of individual California rainfall events shows that not all El Niño events favor heavy rainfall (e.g., [Mo and Higgins 1998](#)). In addition to enhanced convection in the central tropical Pacific, convection in the subtropical eastern Pacific may need to be suppressed during an El Niño event for California to experience wet conditions (e.g., [Mo and Higgins 1998](#)).

A number of recent studies have focused specifically on the unexpectedly low SOCAL rainfall during the winter of 2015/16. [Wanders et al. \(2017\)](#) have evaluated the performance of the January–March North American Multi-Model Ensemble (NMME; [Kirtman et al. 2014](#)) forecasts for the 1982–2010 period and the 2015/16 El Niño event. Rather than a difference in El Niño characteristics they attribute the NMME’s exceptionally poor skill for 2016 California winter precipitation anomalies to atmospheric blocking and the resulting atmospheric circulation patterns that differed from the canonical El Niño circulation patterns.

[Quan et al. \(2018\)](#) conducted a suite of experiments with the Community Atmospheric Model, version 5 (CAM5), in which the atmosphere was forced with the observed sea surface temperature (SST) patterns for the 1982/83 and 2015/16 El Niño events. They found that while the ensemble-mean precipitation was somewhat reduced over California for 2015/16 relative to 1982/83, rainfall was significantly above average in both sets of experiments. Interestingly, additional experiments found that differences in the geographic distribution of the SST anomalies (i.e., maximum SST in the central versus eastern Pacific) did not cause the observed PNA-like circulation pattern differences. Instead, they ascribe the differences to surface boundary conditions outside of the Pacific. This finding is arguably at odds with all the studies cited above attributing a strong role to ENSO flavor and persistence.

In contrast to [Quan et al. \(2018\)](#) and [Wanders et al. \(2017\)](#), [Siler et al. \(2017\)](#) found that many of the differences among the ensemble-mean California rainfall for the 2015/16, 1982/83, and 1997/98 events could in fact be explained by differences in boundary forcing. They conducted a suite of experiments with the

Geophysical Fluid Dynamics Laboratory Atmospheric Model v2.1 (GFDL AM2.1) and identified a non-ENSO pattern of SST in their simulations that was negatively correlated with rainfall across California. An index of this pattern, which is associated with the third empirical orthogonal function (EOF) of tropical outgoing long-wave radiation (OLR) and has its maximum amplitude in the eastern Indian Ocean [see Fig. 5i in Siler et al. (2017)], was even more strongly correlated with California rainfall in their simulations than Niño-3.4 [see Table 1 in Siler et al. (2017)]. By adding or subtracting this pattern from the forcing SST fields they were able to drastically alter the ensemble-mean precipitation response for California. Although the authors acknowledge that this pattern is unlikely to represent a physical mode of the system, due to its high order and low explained variance, its striking impact on the ensemble-mean precipitation in their simulations suggested a previously overlooked and potentially predictable element to the 2015/16 event.

Given that the large El Niño events in 1982/83 and 1997/98 did lead to increased SOCAL rainfall whereas 2015/16 did not, it is natural to question whether this relationship has weakened over time. Previous studies have noted apparent decadal shifts in the relationship between ENSO and precipitation in the Indian, west Pacific, and East Asian monsoons (e.g., Kumar et al. 1999; Kwon et al. 2005; Chen and Zhou 2014). Other studies, however, have noted that these changes in correlation are indistinguishable from sampling variability (Gershunov et al. 2001; DelSole and Shukla 2012; Cash et al. 2017). McCabe and Dettinger (1999) suggest that decadal modes of tropical and North Pacific climate variability can influence the strength of the teleconnection between El Niño and Californian rainfall, while Quan et al. (2018) evaluate the effect of global warming on the teleconnection between El Niño and Californian rainfall by constructing composites of El Niño events occurring within 15-yr periods centered on 1983 and 2016 in a 40-member AOGCM simulation that reproduces the observed global warming trend, they find that the lack of Californian rainfall during the 2015/16 El Niño cannot be attributed to a global warming-induced change in the teleconnection between El Niño and California rainfall.

In the current work, we expand upon these previous studies by exploring the different factors influencing West Coast rainfall in both models and observations. We examine the predicted (forced) and unpredicted (unforced) elements of SOCAL and PNW rainfall in the NMME, a multimodel suite of coupled operational forecasts. We exploit the information available in the large number of individual ensemble members to assess quantitatively the relative impact of forced and

unforced variability on West Coast rainfall. We find that ensemble means, including the multimodel ensemble mean (MMEM), generally overemphasize the influence of El Niño, and that the majority of both Southern California and Pacific Northwest rainfall is associated with unpredicted variability. We show that this rainfall variability is strongly associated with variations in geopotential heights off the West Coast of the United States, and that this same feature figured prominently in the anomalous winter of 2015/16. Improving prediction of these variations thus represents a key target for improving seasonal rainfall predictions for this region.

## 2. Data and methodology

### a. Data

As noted in the introduction, we analyze the role of both predicted and unpredicted variations in determining rainy season precipitation for SOCAL and PNW within coupled models. To do so we make use of the large number of individual models and ensemble members available from the NMME, which is a multimodel, multi-institution forecast product that was in use operationally during the 2015/16 event. The NMME data catalog also includes hindcasts for the period 1982–2009, and thus encompasses the previous high-amplitude 1982/83 and 1997/98 El Niño events. We analyze here the subset of the NMME runs initialized 1 October whose output data of predicted SST, precipitation, and 200-hPa heights ( $z_{200}$ ) have been made available through the International Research Institute data library (see Table 1) for the November–March (NDJFM) period, during which the majority of the rainfall in our target region occurs.

In addition to data from the NMME we also analyze observational data from the Climate Prediction Center (CPC) Unified Precipitation product (CPC-Uni; Xie et al. 2007; Chen et al. 2008), the CPC Merged Analysis of Precipitation (CMAP; Xie and Arkin 1997), and the Extended Reconstructed v4 Sea Surface Temperature (ERSST) product (Huang et al. 2015a,b).

### b. Methodology

In our analysis we take advantage of the information available in the individual ensemble members of the NMME to assess the relative importance of predicted and unpredicted climate variations on the relationship with El Niño. For each model and ensemble member, we decompose model fields into two components; for example,  $SST_{ij} = SST_i^E + SST_{ij}^N$ , where  $SST_{ij}$  is the total SST field for season  $i$  and member  $j$ ,  $SST_i^E$  is the ensemble mean for season  $i$ , and  $SST_{ij}^N$  is the deviation of a given ensemble member from the ensemble

TABLE 1. Included NMME models (expansions of acronyms are available online at <http://www.ametsoc.org/PubsAcronymList>). Notations such as 0.25°Eq indicate the model's resolution at the equator.

Model	Hindcast period	Ensemble size	Forecast lead (months)	Native atmosphere resolution	Native ocean resolution	Reference
NCEP-CFSv2	1982–2010	24	0–9	T126L64	MOM4L40 0.25°Eq	<a href="#">Saha et al. (2014)</a>
GFDL-CM2p1 aer04	1982–2010	10	0–11	2° × 2.5°, L24	MOM4L50 0.3°Eq	<a href="#">Delworth et al. (2006)</a>
GFDL-CM2p5 FLORB01	1982–2010	12	0–11	C18L32 (50 km)	MOM4L50 0.3°Eq	<a href="#">Vecchi et al. (2014)</a>
GFDL-CM2p5 FLORA06	1982–2010	12	0–11	C18L32 (50 km)	MOM4L50 0.3°Eq	
CMC1-CanCM3	1982–2010	10	0–11	T63L31	CanOM4L40 0.94°Eq	<a href="#">Merryfield et al. (2013)</a>
CMC2-CanCM4	1982–2010	10	0–11	T63L315	CanOM4L40 0.94°Eq	
NCAR-CCSM3 (COLA-RSMAS)	1982–2010	6	0–11	T85L26	POPL42 0.3°Eq	<a href="#">Kirtman and Min (2009)</a>
NCAR-CCSM4 (COLA-RSMAS)	1982–2010	10	0–11	0.9° × 1.25°, L26	POPL60 0.25°Eq	<a href="#">Infanti and Kirtman (2016)</a>
NASA-GMAO-062012	1982–2010	11	0–11	1° × 1.25°, L72	MOM4L40 0.25°Eq	<a href="#">Vernieres et al. (2012)</a>

mean.  $SST_i^E$  is the component of SST that is common to all of the ensemble members, and is therefore the portion of the SST field that the model reproduces regardless of small changes in initial conditions. We refer to this component as the *predicted* or *forced component*.  $SST_{ij}^N$  is then the difference between a single ensemble member and the ensemble mean, representing the component of the model field that is sensitive to initial conditions. We refer to it here as the *unpredicted component* or simply *noise*. Note that both the predicted and unpredicted components are defined for each model and variable separately and are explicitly both model and variable dependent.

Using this decomposition, we can assess the contribution from the different components to relationships in each model. For example, the linear correlation between the ensemble mean of SST and Southern California rainfall is given as

$$\rho_E = \frac{\sum SST^E SOCAL^E}{\sqrt{\sum (SST^E)^2} \sqrt{\sum (SOCAL^E)^2}} \quad (1)$$

while the correlation between the noise is

$$\rho_N = \frac{\sum SST^N SOCAL^N}{\sqrt{\sum (SST^N)^2} \sqrt{\sum (SOCAL^N)^2}}. \quad (2)$$

The total correlation between SST and SOCAL rainfall can then be expressed through a combination of these two components, only now they are normalized by the

product of the total standard deviation of each term (e.g.,  $SST^A$  and  $SOCAL^A$ ):

$$\rho_A = \frac{\sum (SST^E + SST^N)(SOCAL^E + SOCAL^N)}{\sqrt{\sum (SST^A)^2} \sqrt{\sum (SOCAL^A)^2}}.$$

Since the cross-covariance between the noise and ensemble terms is negligible (not shown), the total correlation reduces to

$$\begin{aligned} \rho_A &= \frac{\sum (SST^E SOCAL^E + SST^N SOCAL^N)}{\sqrt{\sum (SST^A)^2} \sqrt{\sum (SOCAL^A)^2}} \\ &= \frac{\sum SST^E SOCAL^E}{\sqrt{\sum (SST^A)^2} \sqrt{\sum (SOCAL^A)^2}} \\ &\quad + \frac{\sum SST^N SOCAL^N}{\sqrt{\sum (SST^A)^2} \sqrt{\sum (SOCAL^A)^2}}. \end{aligned} \quad (3)$$

Thus, the total correlation between the two quantities within each model's ensemble can be expressed in terms of separate contributions from the predictable and unpredictable components, normalized by the product of the total standard deviation of each term ( $SST^A$ ,  $SOCAL^A$ ). Note that this normalization is different from that obtained from the sum of (1) and (2). We can use this decomposition to assess the relative contribution of predicted and unpredicted components to the total correlation. For the 28 samples in the period 1982–2009, for both observations and  $\rho_E$  a value of 0.375 is

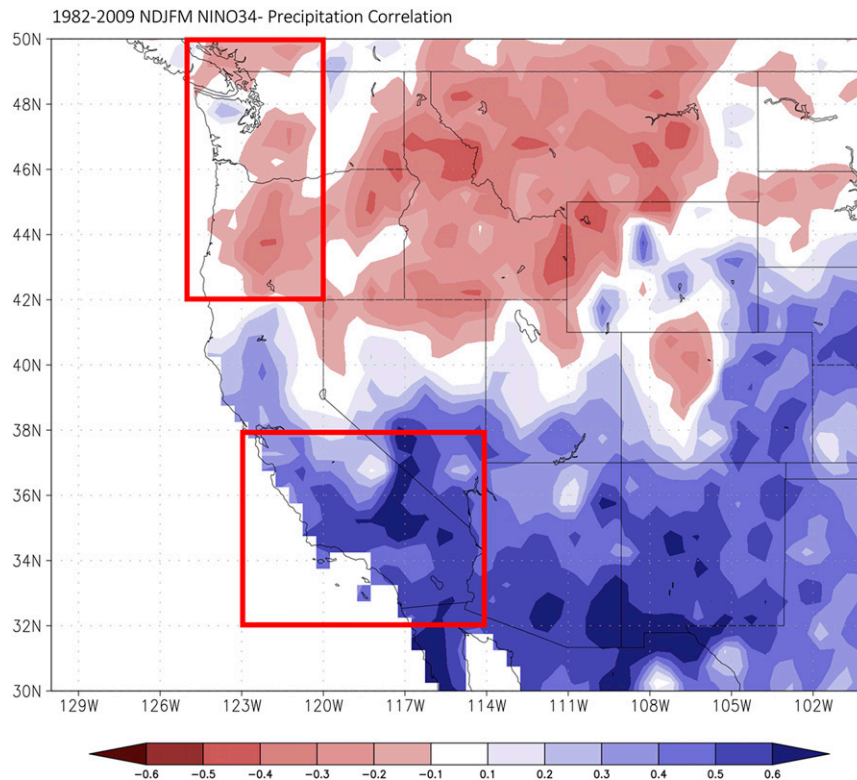


FIG. 1. Correlation between the Niño-3.4 index and precipitation for NDJFM for the period 1982–2009. SST data are from ERSSTv4; precipitation data are from CPC Unified. Heavy red outlines denote boundaries of PNW and SOCAL regions used in this study.

significant at the 95% level in a two-tailed test. For the much larger set of samples used to calculate  $\rho_A$  and  $\rho_N$  any value displayed is statistically significantly different from zero, if not necessarily physically significant.

### 3. Results

#### *a. Local and remote associations with West Coast rainfall*

We first calculate the correlation between the NDJFM CPC-Uni rainfall in the western continental United States and the Niño-3.4 index at each grid point for the same base period of 1982–2009 (Fig. 1a), as a means of assessing the general strength of the linear association between ENSO and rainfall. The correlation map shows a clear north–south dipole pattern, with negative correlations (dry conditions) across the Pacific Northwest and positive correlations (wet conditions) extending from Southern California across the American Southwest and northern Mexico. Magnitudes in Southern California generally range from 0.4 to 0.6, which are significantly different from zero for a sample of 28 years at the 95% level (magnitude greater than 0.375 for a two-tailed test).

Despite the fact that there are significant correlations between Niño-3.4 and SOCAL rainfall, even the peak value of  $\sim 0.6$  in Fig. 1a only explains  $\sim 36\%$  of the total variance. The amount of NDJFM SOCAL precipitation variance explained by Niño-3.4 is generally closer to 20%. Thus, while there is clearly a positive relationship between SOCAL rainfall and El Niño in the observations, it explains less than half of the observed seasonal variability. In Northern California the relationship is much weaker, generally falling below statistical significance and explaining less than 10% of the variance. The correlation between Niño-3.4 and the Pacific Northwest is negative and also statistically significant, but again the variance explained is generally around 20%.

While the correlation map indicates the general response to El Niño events in the western United States is increased rainfall to the south and reduced rainfall to the north, it is important to note that even the strongest individual events in the recent period (1982/83, 1997/98, 2015/16) show significant deviations from this “canonical” pattern. During the 1982/83 event rainfall increased along the entire U.S. West Coast, including the canonically dry northwest region, with the maximum anomaly centered in Northern California (Fig. 2a). While rainfall did increase



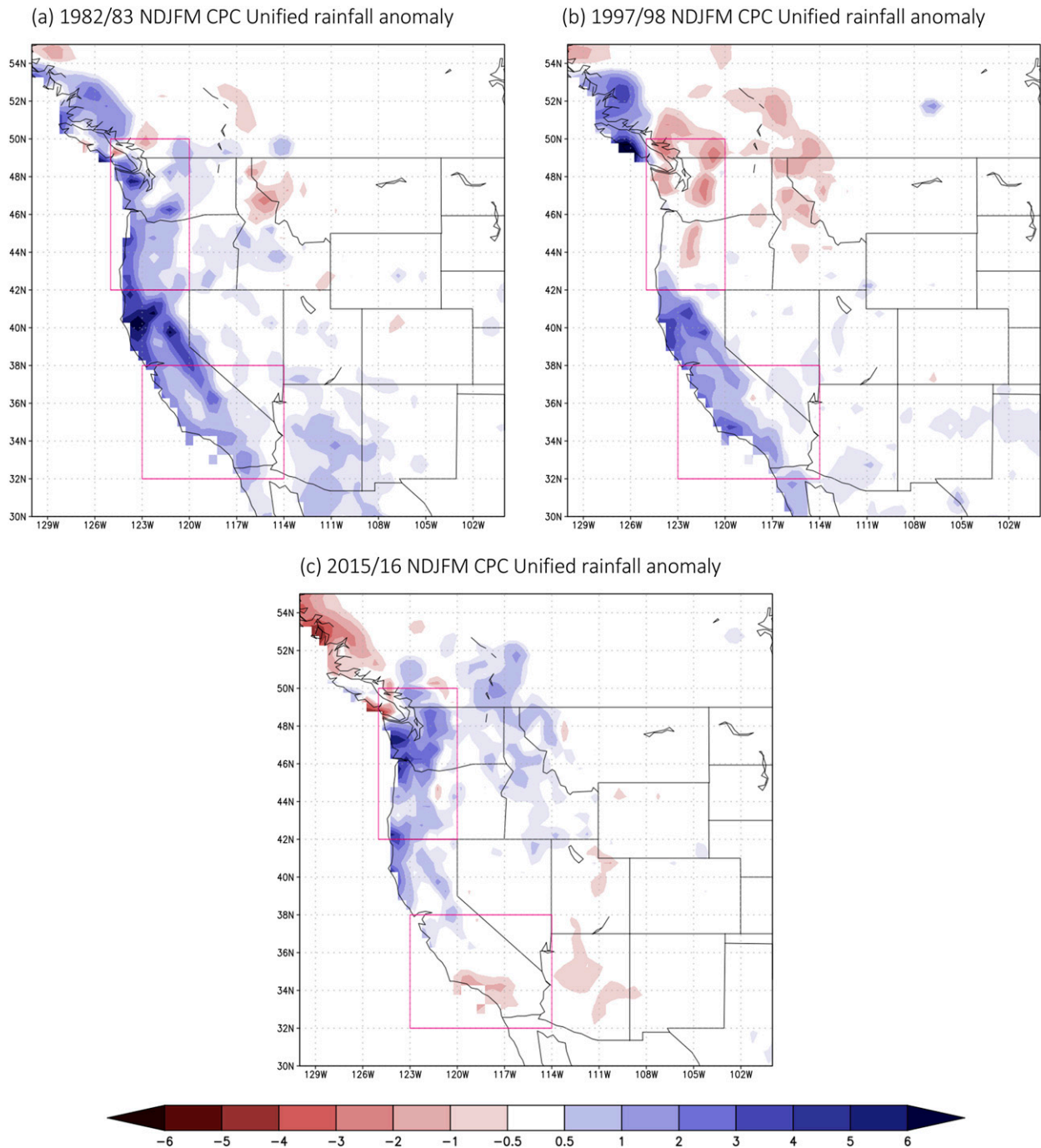


FIG. 2. Observed precipitation anomaly ( $\text{mm day}^{-1}$ ) from CPC Unified data for NDJFM for (a) 1982/83, (b) 1997/98, and (c) 2015/16.

in Southern California, the anomaly pattern bore little resemblance to the general relationship (Fig. 1a). The 1997/98 NDJFM rainfall anomaly (Fig. 2b) most closely resembles the Niño-3.4 correlation pattern, with dry anomalies in the northern part of the domain and wet anomalies to the south. However, the anomalies outside of California were relatively weak and the anomaly in

Northern California comparatively too strong. Finally, as noted in the introduction, the 2015/16 event (Fig. 2c) produced a near reversal of the correlation pattern, with wet anomalies to the north and dry anomalies to the south.

The observed response of West Coast precipitation to recent large El Niño events has thus been highly variable

and often contrary to the correlation pattern, with dry anomalies in California during 2015/16 and wet anomalies in the Pacific Northwest in two out of the three events. The simulated ensemble-mean responses to the major El Niño events, on the other hand, are fairly consistent, particularly for SOCAL (Fig. 3).

For the 1982/83 event (Fig. 3a), the NMME hindcast of Southern California rainfall (the southern area delineated by a red box in Fig. 1) has the MMEM (dashed black line) predicting above-average rainfall for the entire NDJFM period. The distribution of individual ensemble members (colored bars) shows a strong skewness toward positive values, as expected for a positive-definite quantity like rainfall, in addition to having more positive members than negative. However, it is worth noting that even during the period with the strongest wet anomalies in the MMEM (January–March) there are still members with dry anomalies, demonstrating a sensitivity to initial conditions among the individual runs. For the PNW (the northern red box in Fig. 1), the MMEM hindcast is below average for all of the winter months, consistent with the El Niño association but opposite to what was observed (Fig. 3a).

The model representation of the 1997/98 event for SOCAL (Fig. 3c) is very similar to that of 1982/83, with above-average MMEM values and a nontrivial number of dry members. It is worth noting that the MMEM does not show any signature of the extreme rainfall that occurred in February, nor do any of the individual model's ensemble means. This illustrates that the predictable components of the models may not capture all aspects of the wet El Niño event even when getting the sign correct. Somewhat surprisingly the PNW hindcast for 1997/98 (Fig. 3d) indicated, incorrectly, near-normal to slightly above-normal conditions, despite the strong El Niño event.

Finally, for the 2015/16 event the MMEM for SOCAL (Fig. 3e) was essentially unchanged from the 1982/83 and 1997/98 events, despite the large observed differences. The MMEM is again above normal, and the models uniformly fail to capture the large February dry anomaly. The MMEM also predicted below-average precipitation for the PNW (Fig. 3f), consistent with the correlation pattern but opposite to what was observed. While the MMEM for SOCAL in 2015/16 is somewhat drier than for the previous events, consistent with Quan et al. (2018) and Siler et al. (2017), the model response is largely indistinguishable from that of the previous wet years.

Taken together, the NMME hindcasts for 1982/83, 1997/98, and 2015/16 suggest that the general association between Niño-3.4 and rainfall along the U.S. West Coast is too strong and too consistent in the MMEM, leading

to significant errors for SOCAL in 2015/16 and the PNW in both 1982/83 and 2015/16. To test this hypothesis, we compare the correlation between Niño-3.4 and precipitation calculated over all members in the NMME, thus retaining the influence of noise [Fig. 4a;  $\rho_A$  in Eq. (3)], to the correlation calculated using just the MMEM [Fig. 4b;  $\rho_E$  in Eq. (1)]. We find that when the individual members are used the correlation values are relatively similar to the observations in both pattern and magnitude (cf. Figs. 1 and 4a). While the correlation pattern for the MMEM (Fig. 4b) also produces a north–south dipole that is consistent with the observed pattern the magnitudes are much stronger than observed, approaching 1 for some points. *This translates to an unrealistically high percentage of explained variance, with values above 50% for almost all of Southern California and above 90% for portions of the Pacific Northwest.*

Despite the presence of a clear dipole pattern in correlation with Niño-3.4 (Fig. 1), the differences in the PNW and SOCAL regions for the recent large events (Figs. 2 and 3) suggest that the anticorrelation between the PNW and SOCAL is potentially not as strong as Fig. 1 would suggest when looking across all years. To test this hypothesis, we calculate the correlation between the PNW and SOCAL indices and U.S. rainfall separately (Fig. 5). The correlation map for the PNW (Fig. 5a) shows a distinct dipole similar to Fig. 1, but the node of the dipole lies farther south and cuts directly through the SOCAL box. For the SOCAL index (Fig. 5b) the similarity to the Niño-3.4 correlation map (Fig. 1) is much reduced, with only relatively weak negative correlations across the northwest region. As suggested by Fig. 5 the correlation between the PNW and SOCAL indices is negative but weak ( $-0.1$ ), indicating that the association between the regions is significantly weaker than the correlation with Niño-3.4 would imply.

The differences in behavior between the PNW and SOCAL regions becomes more apparent in their relationship with SST (Fig. 6). Correlating PNW rainfall against SST (Fig. 6a) yields a relatively weak La Niña pattern in the tropical Pacific and negative correlations across the Indian Ocean and tropical Atlantic. It should be noted that extending the domain considered for the PNW eastward increases the magnitude of the correlation with the tropical Pacific (as we would expect from Fig. 1), but our focus here is on the region of maximum rainfall anomalies in 2015/16 (Fig. 2c). Correlating SOCAL rainfall against SST (Fig. 6b), however, produces a map that closely resembles the classic El Niño SST anomaly pattern. In light of the Siler et al. (2017) results discussed in the introduction, it is worth noting that while there are correlation magnitudes above 0.3 in the Indian Ocean

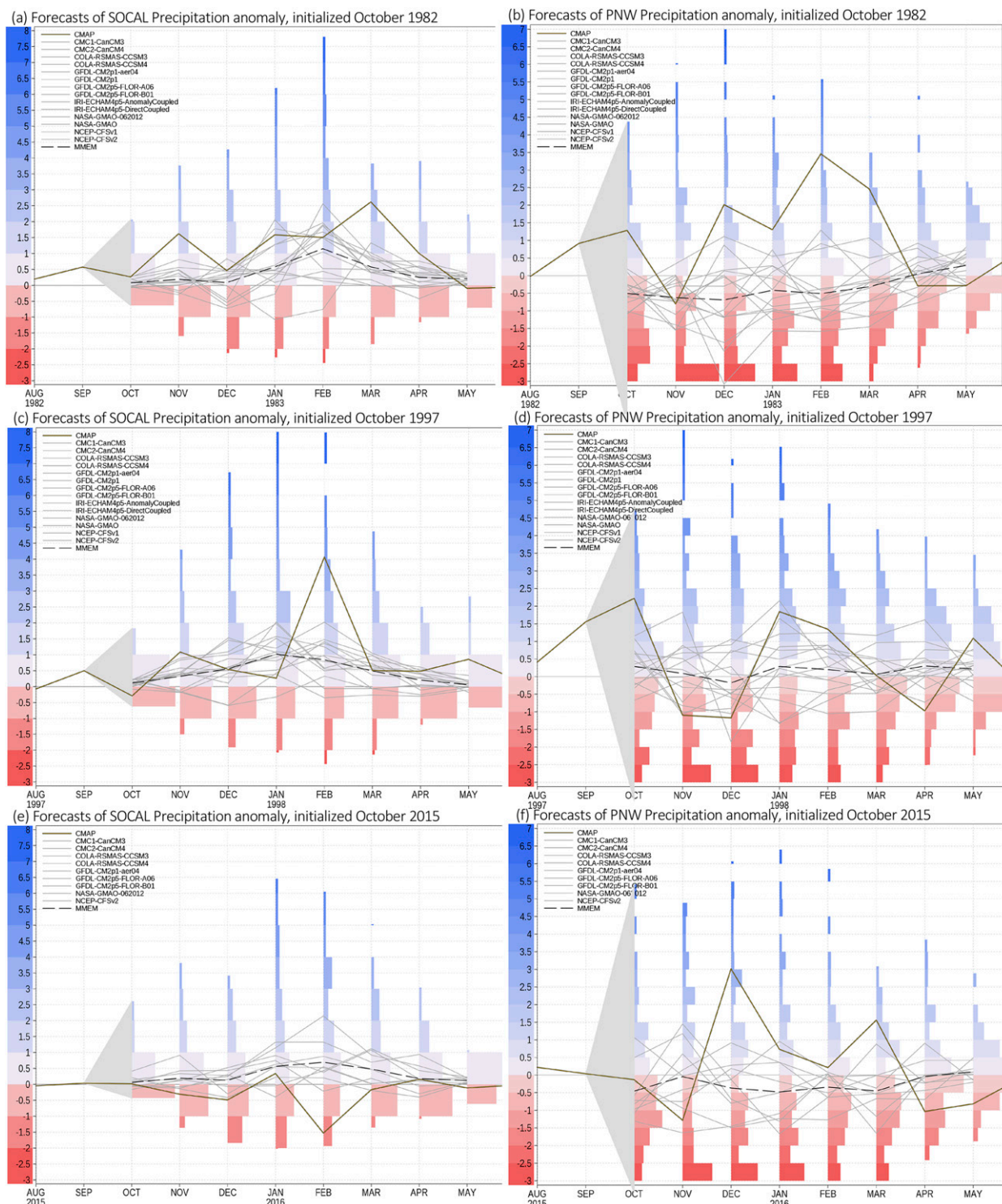


FIG. 3. Seasonal forecasts of (left) SOCAL and (right) PNW rainfall anomalies ( $\text{mm day}^{-1}$ ) from NMME initialized (a),(b) 1 Oct 1982, (c),(d) 1 Oct 1997, and (e),(f) 1 Oct 2015. Gray lines denote individual model ensemble means. Dashed line denotes MMEM. Heavy solid line denotes the observed anomaly from CMAP. Colored bars represent histogram of anomalies from individual members, as denoted by the left-hand-side vertical axis.



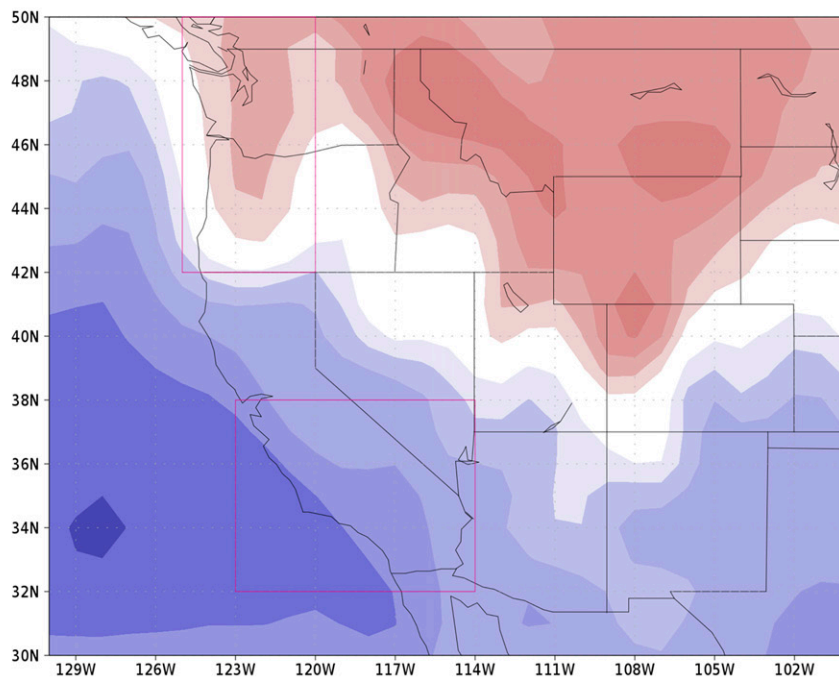
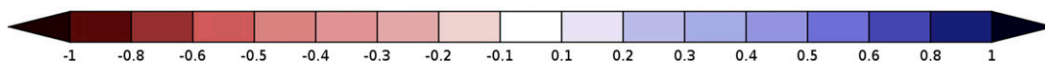
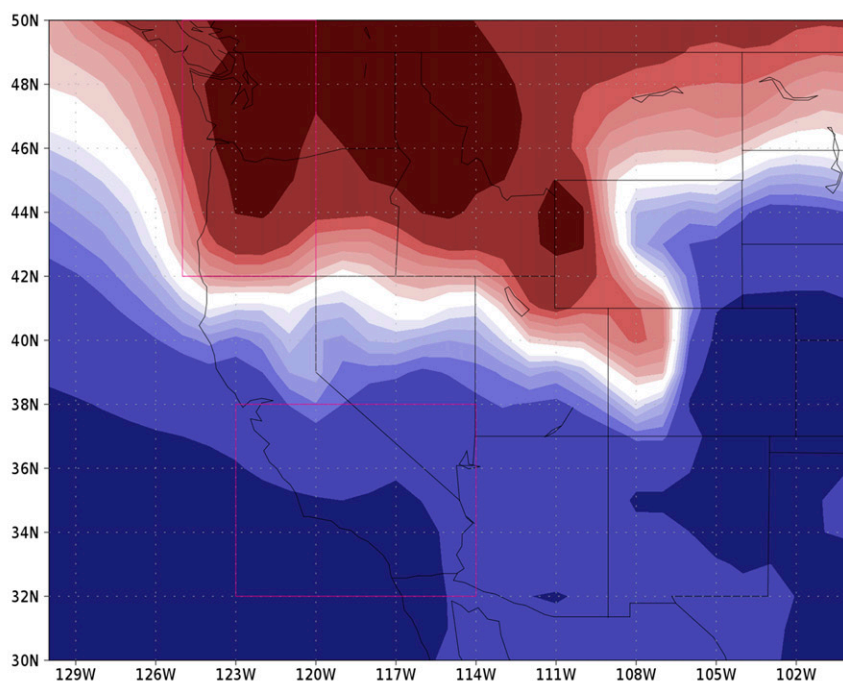
(a)  $\rho_A$ : MME NINO34 – Precip correlation. 1982-2009, NDJFM, October initialization(b)  $\rho_E$ : MME NINO34 – Precip correlation. 1982-2009, NDJFM, October initialization

FIG. 4. Model correlation between the Niño-3.4 index and precipitation for (a) MME and (b) MME Niño-3.4 and precipitation for NDJFM for the period 1982–2009.

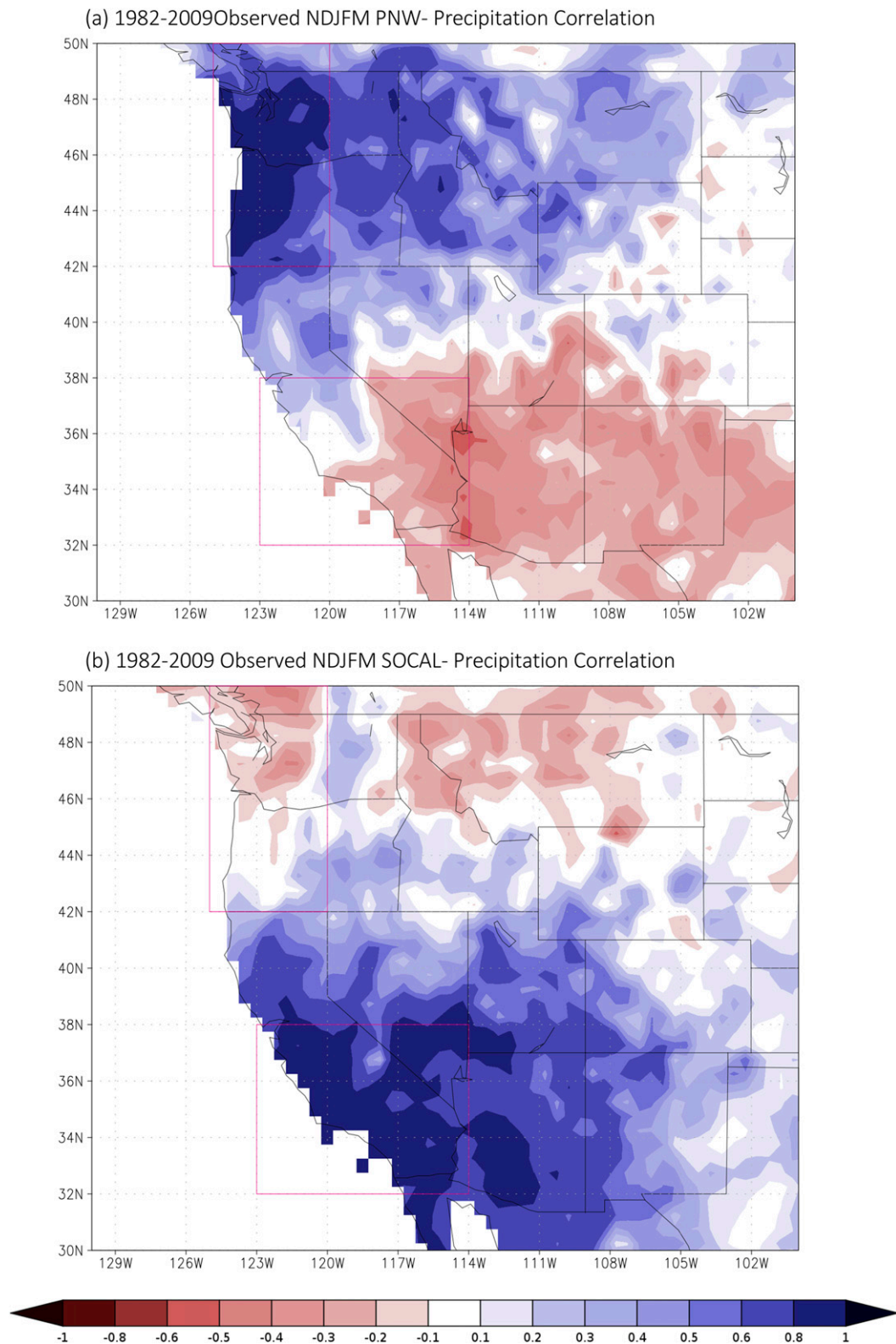


FIG. 5. Observed correlation between the (a) PNW and (b) SOCAL indices and U.S. precipitation for NDJFM for the period 1982–2009.

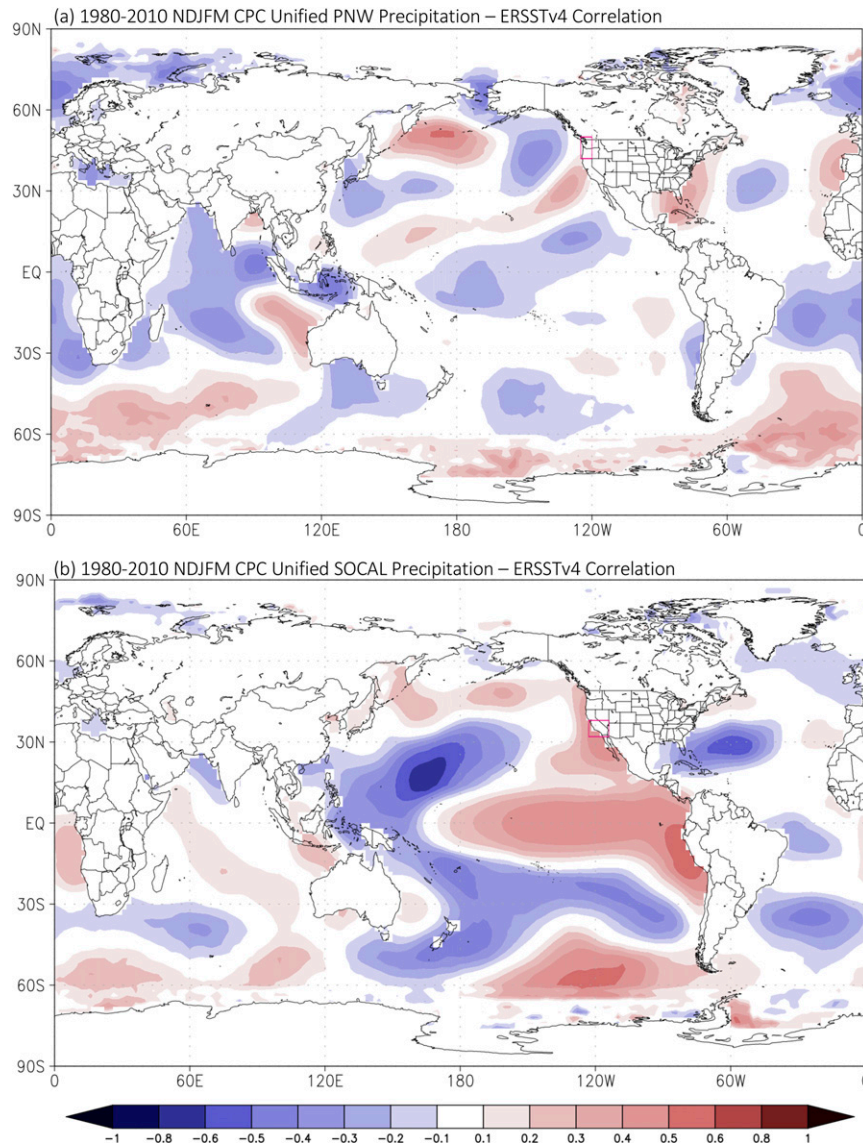


FIG. 6. Correlation between (a) PNW and (b) SOCAL precipitation and SST for NDJFM for the period 1982–2009. SST data are from ERSSTv4; precipitation data are from CPC Unified.

for the PNW index, SOCAL correlations for the Indian Ocean are near zero and are not statistically significant.

Turning our attention to the relationship between PNW rainfall and SST in the models, we find that calculating the correlation over all members produces very little in the way of significant correlations (Fig. 7a). The observed feature in the Gulf of Alaska seen in Fig. 6a is captured by the models, as is the suggestion of the La Niña pattern in the tropical Pacific (although weaker). However, when the ensemble-mean quantities are used [ $\rho_A$  in Eq. (3)], the correlation pattern changes dramatically (Fig. 7b). The tropical Pacific is now dominated by highly significant correlations in a classic ENSO

“horseshoe” pattern. The strong negative correlations across the central and eastern equatorial region indicate that in the ensemble mean the PNW rainfall responds far more strongly than observed to presence of an ENSO event.

As with the PNW, calculating the correlation between SOCAL rainfall and SST over all members [Fig. 8a;  $\rho_A$  in Eq. (3)] produces a remarkably similar pattern to the observations (cf. to Fig. 6b), both in terms of spatial extent and magnitude. Unlike the PNW the association with the tropical Pacific is quite apparent even when the unpredicted elements are retained, suggesting that the association between the tropical Pacific and rainfall is



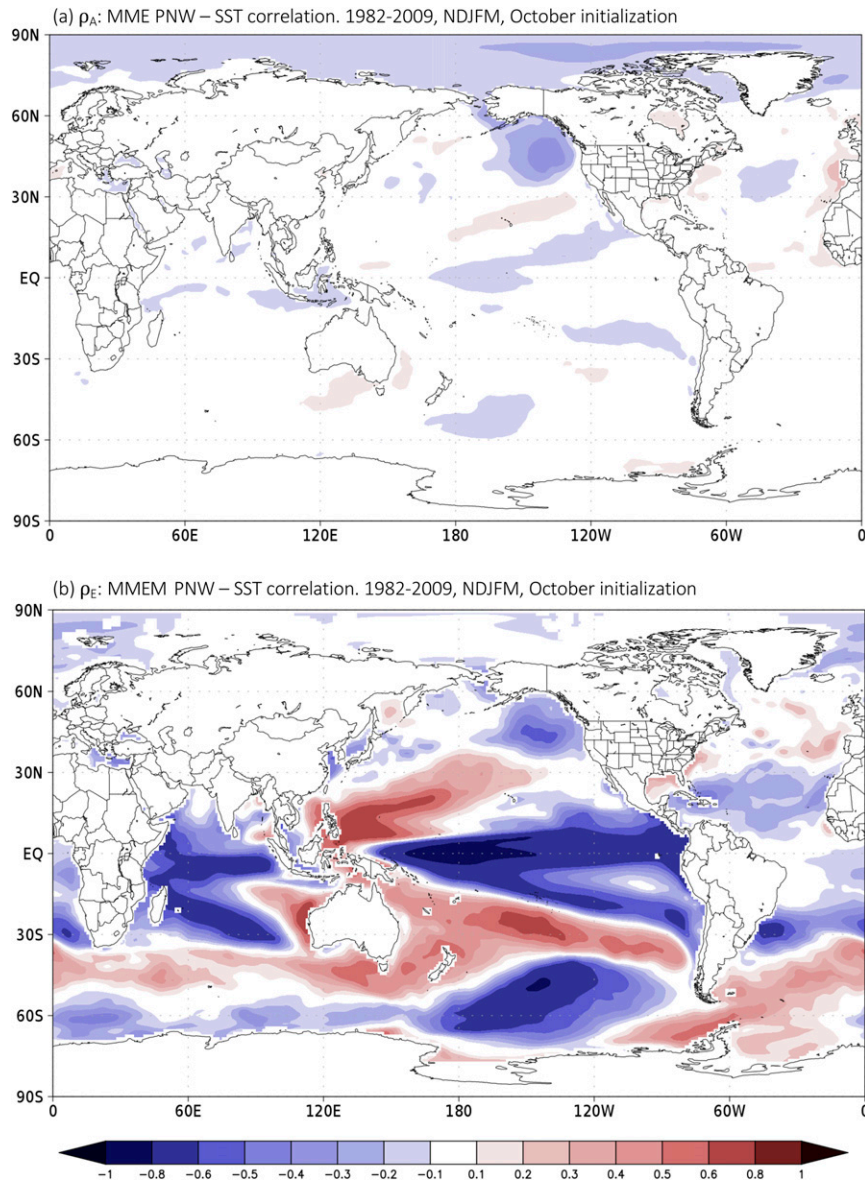


FIG. 7. Correlation between PNW index and SST for (a) MME and (b) MMEM Niño-3.4 and precipitation for NDJFM for 1982–2009.

stronger and less dominated by noise in the southern part of the region.

As with the PNW, correlating the MMEM SOCAL rainfall and MMEM SST [Fig. 8b;  $\rho_N$  in Eq. (1)] produces significantly higher magnitudes than are observed around the globe. Statistically significant correlations are found for almost all tropical grid points, as well as for numerous points in the extratropics. Interestingly, the positive correlations extend farther west in the tropics in the MMEM than for the observations or total correlation (Figs. 8a and 6b, respectively), suggesting a stronger coupled model SST bias in the western tropical Pacific

than would be inferred from the  $\rho_A$  calculation. The ensemble-mean correlation maps for the PNW and SOCAL rainfall and SST are also near-reverse images (cf. Figs. 7b and 8b), suggesting that the relationship with SST is significantly more linear in the ensemble mean than it is in the full model or the observations.

The similarity between the correlation maps using the full ensemble and the observations suggests that the coupled models are doing reasonably well at capturing the observed global relationship when all of the available information is retained. However, it is worth noting that one of the areas of greatest difference between the models



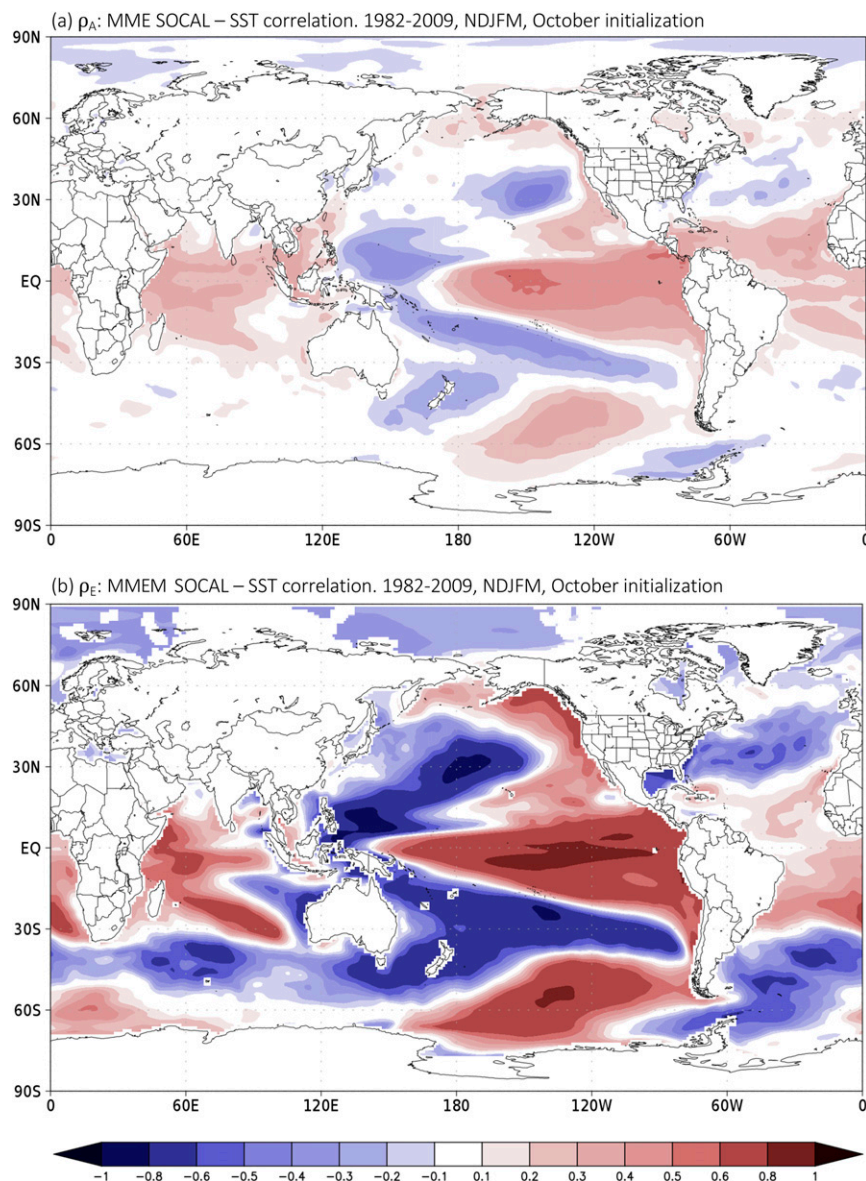


FIG. 8. Model correlation between SOCAL index and SST for (a) MME and (b) MMEM Niño-3.4 and precipitation for NDJFM for 1982–2009.

and observations is in the Indian Ocean, where the models overestimate the strength of the correlation with Southern California rainfall. This discrepancy may help to explain the difference between the results of Siler et al. (2017; see their Table 1 and Fig. 5i) and the observed correlation shown in Fig. 1b.

Turning our attention to the atmospheric patterns, the association between West Coast rainfall and 200-hPa heights generally follows the same pattern as SST for both the observations (Fig. 9) and the NMME (Fig. 10). In the observations, PNW rainfall is strongly correlated with negative 200-hPa height anomalies along

the Canadian west coast (Fig. 9a), as well as positive height anomalies over Southern California. Correlations with the tropics are generally negative and weak, consistent with the weak association with tropical SST. The correlation with SOCAL rainfall (Fig. 9b), in contrast, shows a strong correlation with positive height anomalies over the central and eastern tropical Pacific, with strong negative associations in the north and South Pacific associated with a wave train-like pattern. Comparing the patterns for the two indices (Figs. 9a and 9b) we find that the negative correlation near California for the SOCAL index is shifted slightly north relative to the

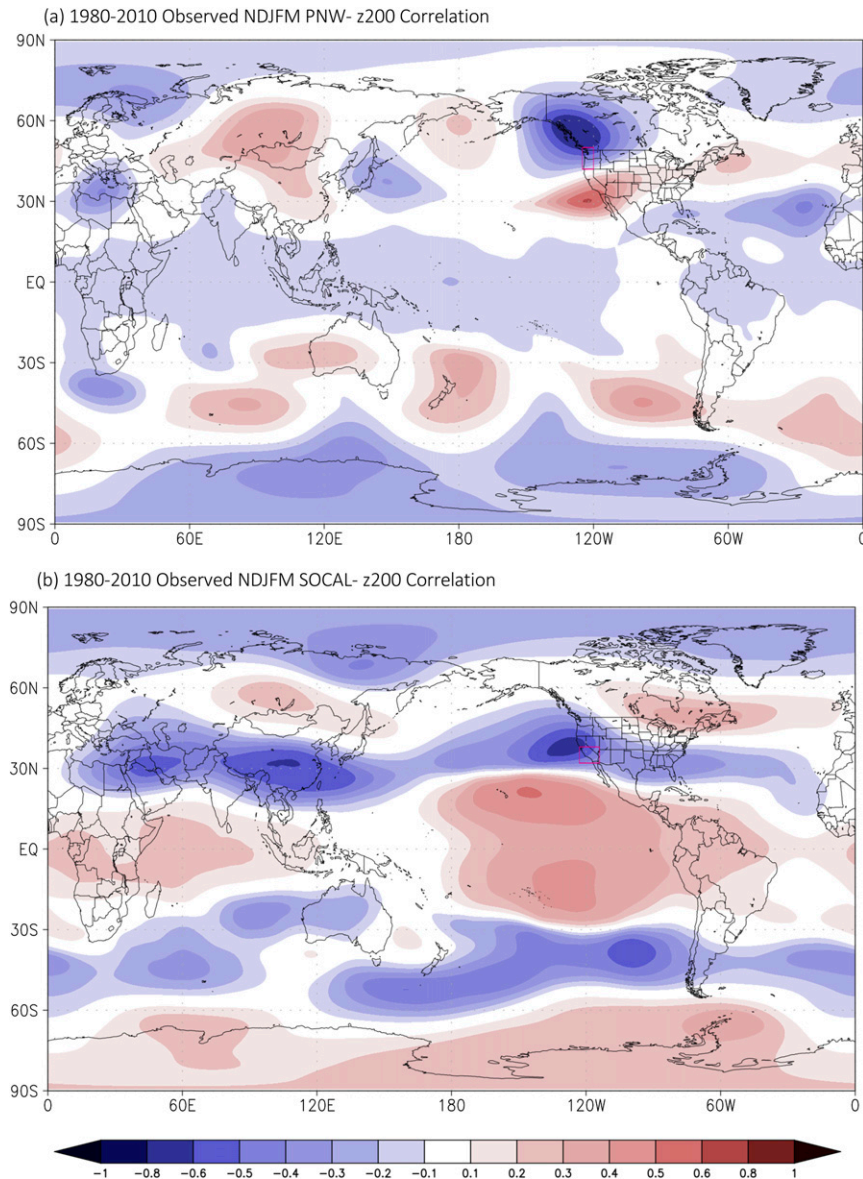


FIG. 9. Observed correlation between the (a) PNW and (b) SOCAL indices and z200 for observations for NDJFM for the period 1982–2009.

corresponding (positive) PNW center, and that the center over Canada is not present. The patterns suggest that PNW is more likely to be associated with rainfall anomalies across the southwest of the United States, due to the strong southern center, while the connection from the SOCAL region to the Pacific Northwest is relatively weak due to the lack of a strong northern center. This is consistent with the relationship indicated in Fig. 5.

As with the comparison between observations and models for SST and precipitation, we find that the total correlation pattern derived from the NMME generally

matches the observed patterns (cf. Figs. 9a and 10a and Figs. 9b and 10b, respectively). While there are differences, particularly over the Arctic and Eurasia for the SOCAL pattern, the models are generally capable of representing the observed relationships to reasonable accuracy.

#### *b. Relative contribution of predicted and unpredicted components*

Having established that the NMME can reproduce the observed association between the PNW and SOCAL rainfall indices and global fields to a reasonable degree,

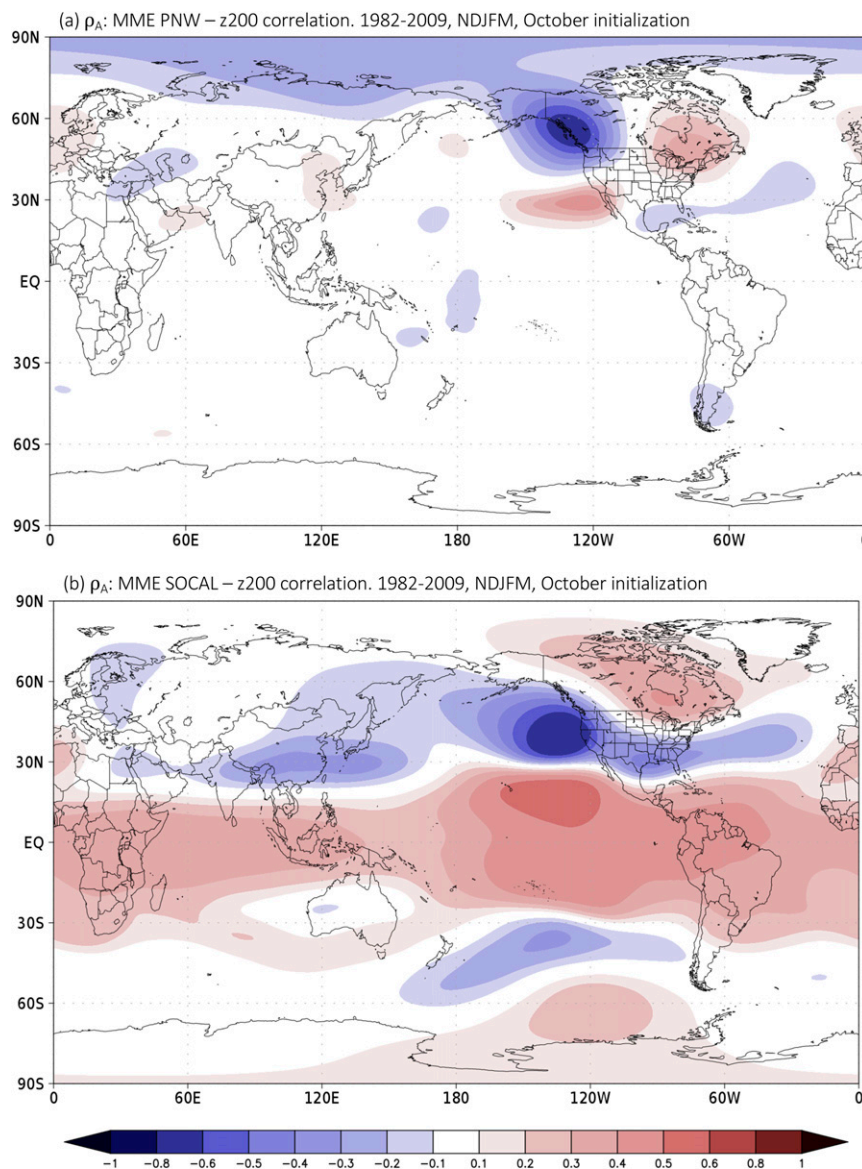


FIG. 10. Model correlation between the (a) PNW and (b) SOCAL indices and z200 for MME for NDJFM for the period 1982–2009.

we can make further use of the decomposition shown in Eqs. (1)–(3) to understand the relative contribution of the predicted and unpredicted components to the total correlation. For SOCAL rainfall and global rainfall (Fig. 11), differences between the two components are immediately apparent. The predicted component (Fig. 11a) is responsible for essentially the entirety of the remote association with the tropical Pacific. The unpredicted component pattern is confined to the west coast of North America, but accounts for by far the majority of the local variability. Thus, while there is a strong association between the predictable components of SOCAL rainfall and SST (Fig. 8b), the predictable

component of rainfall is only a relatively small fraction of the total. The difference is even more dramatic for the PNW index (not shown), as the predictable component of the rainfall is essentially negligible and the unpredicted component accounts for essentially all of the local variability.

Taken together, Figs. 3–11 indicate that while the full NMME can accurately reproduce the observed associations between PNW and SOCAL rainfall and global fields, forecasts focusing on the MME can produce potentially misleading results. The MME represents only that portion of the variability that is reproduced by all of the chosen models (i.e., the predicted component



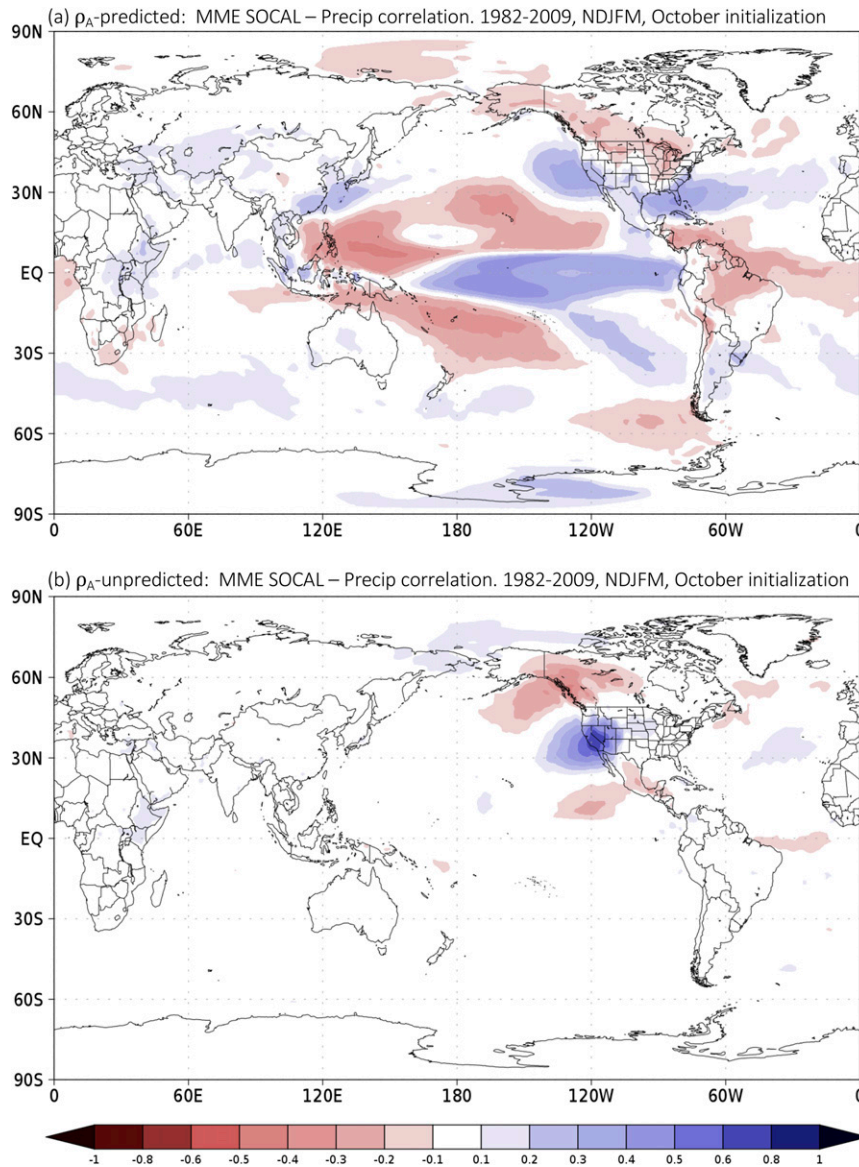


FIG. 11. Contribution to correlation between the MME SOCAL index and precipitation from the (a) predicted and (b) unpredicted components for NDJFM for the period 1982–2009.

of the total variability). While focusing on the MMEM emphasizes the aspects of rainfall that we can predict, it deliberately suppresses the influence of unpredicted variations. Given that ENSO is one of the relatively few aspects of the climate system that can be predicted with any accuracy on seasonal time scales, this has the effect of exaggerating the relationship between West Coast rainfall and ENSO in the NMME MMEM. For those cases where the influence of the unpredicted variability is small or acts to reinforce the ENSO signal the forecast will be relatively accurate. When the noisy component is significant and not aligned with the ENSO

forced component, however, there will be significant potential for a failed forecast. This potential for a failed forecast is particularly high for the PNW region, given how small a fraction of the total variability the ensemble mean actually represents.

### c. Role of unpredicted variability in determining SOCAL rainfall

One possible explanation for the significant unpredicted variations in precipitation is that they are associated with unpredicted variations in SST. For example, higher-than-average SOCAL precipitation could be



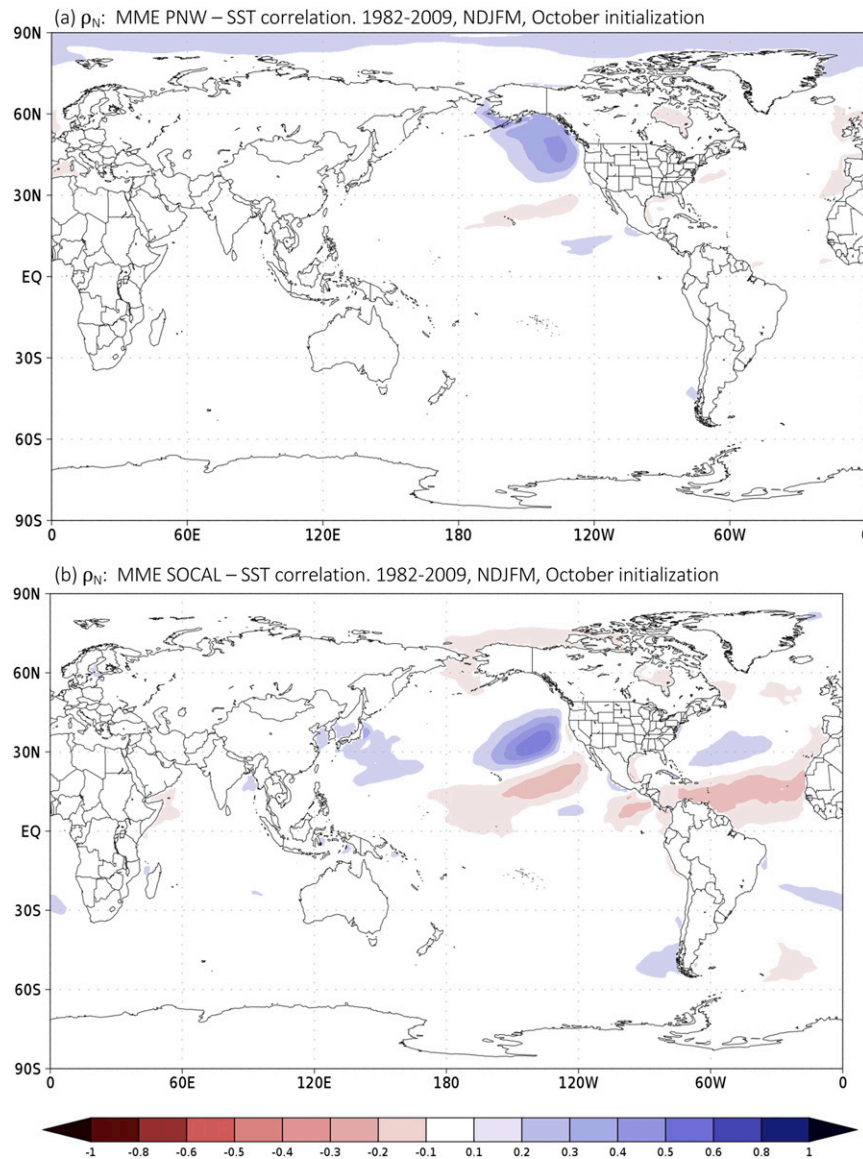


FIG. 12. Correlation between noise (a) PNW and (b) SOCAL indices and noise SST for NDJFM for the period 1982–2009.

paired with a stronger than average El Niño event, or SST anomalies outside of the tropical Pacific. While these anomalies may be currently unpredictable by the NMME, identification of a link between unpredicted variations in SST and PNW precipitation could provide valuable guidance for forecasters as well as scientific insight. However, the correlations between unpredicted rainfall and unpredicted SST [Fig. 12; see Eq. (2)], are generally weak and confined to a region of the North Pacific. For the PNW the maximum correlations are in the Gulf of Alaska region (Fig. 12a), which has been previously identified as potentially influencing winter conditions in the PNW (e.g., Lim et al. 2018).

For SOCAL (Fig. 12b) the anomalies are in a region that is likely to be influenced by circulation changes associated with enhanced rainfall (see below) rather than as a driver. There is no indication of a remote association between, for example, unpredicted variability in the Indian Ocean or tropical Pacific and SOCAL rainfall. Instead, we find that the noise component of precipitation, which dominates both the PNW and SOCAL indices, is determined almost entirely by unpredicted variations in the 200-hPa height field to the immediate west [Figs. 13a and 13b, respectively; Eq. (2)]. The noise components are similar in overall pattern for the two indices but are in near-quadrature, which is consistent

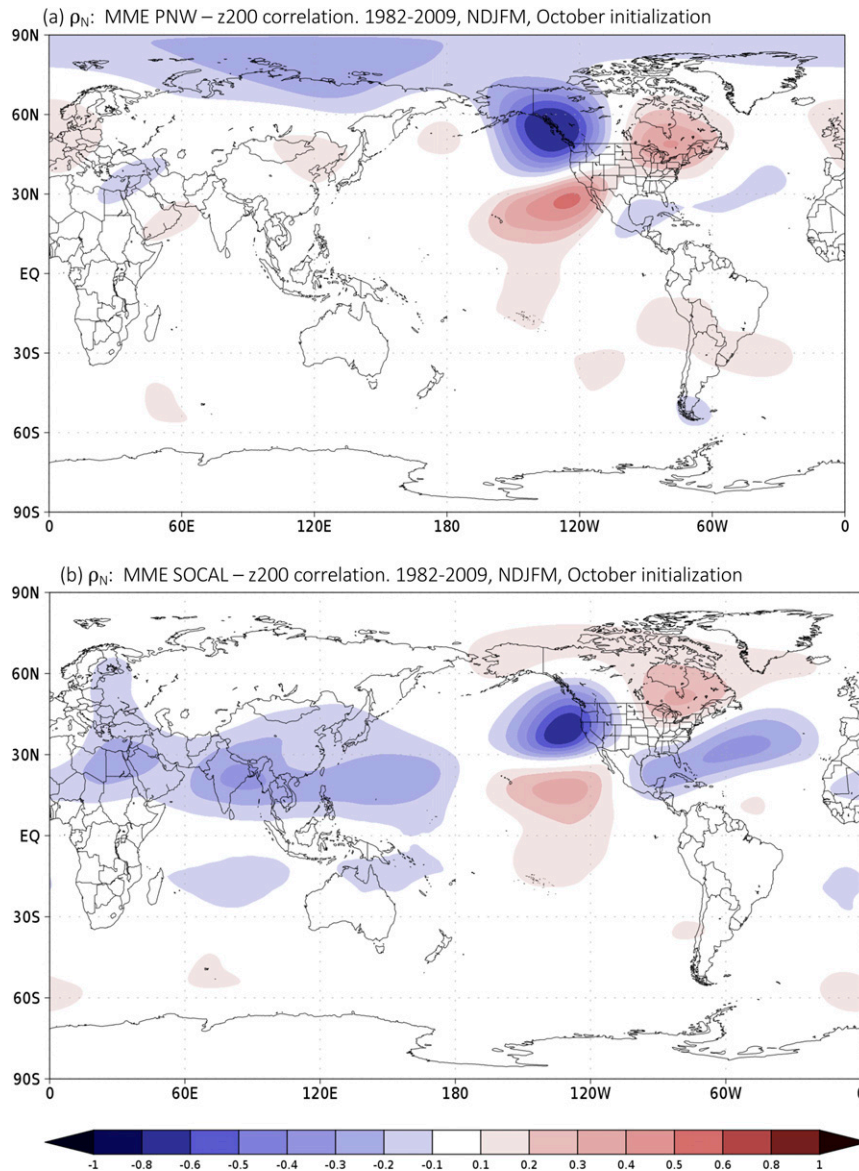


FIG. 13. Model correlation for the unpredicted components of the MME (a) PNW and (b) SOCAL index and z200 for NDJFM for the period 1982–2009.

with the weak correlation between the PNW and SOCAL indices described earlier.

#### d. Understanding the 2015/16 event

Using data for the period 1982–2009 we have shown that, while there is a predictable element to SOCAL rainfall associated with ENSO, the majority of SOCAL rainfall variability is not predictable in the NMME. The predictable component of PNW rainfall is also strongly associated with ENSO but is essentially negligible in terms of the variance explained. Instead both are determined primarily by local, unpredictable fluctuations

in geopotential height (i.e., atmospheric noise) to the immediate north and west of the target region. We now examine the differences between the observed “canonical” response to the 1997/98 El Niño and the “anomalous” response to the 2015/16 event to see whether this general relationship can help to explain the differences between these two specific events.

Comparing the observed rainfall for the two events (Fig. 14), we see significantly drier conditions over California and wetter conditions in the Pacific Northwest in the 2015/16 event, consistent with previous studies. SST anomalies in the 2015/16 event are significantly

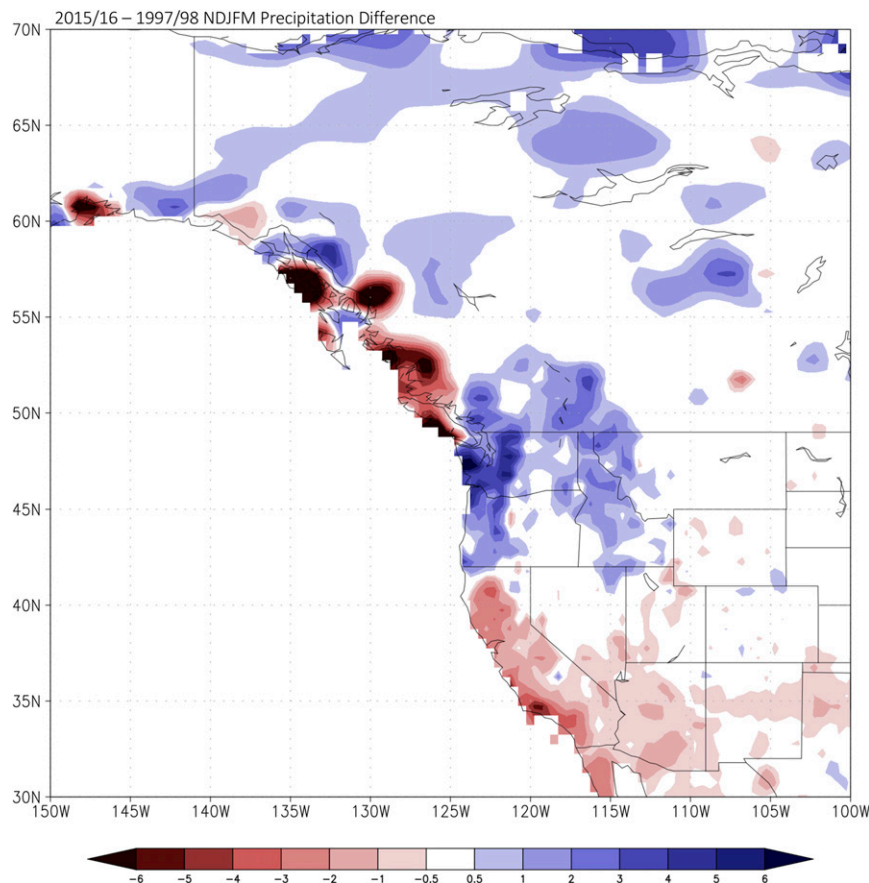


FIG. 14. Observed precipitation difference ( $\text{mm day}^{-1}$ ): NDJFM 2015/16 – 1997/98. Data from CPC Unified.

colder in the eastern tropical Pacific and warmer toward the central Pacific and extratropics (Fig. 15a). The 200-hPa height field (Fig. 15b) is dominated by positive anomalies that cover most longitudes between 30° and 60° latitude in both hemispheres, a pattern that bears a strong resemblance to the inverse of the SOCAL-z200 correlation patterns derived for both the observations and the NMME (Figs. 9b and 10b, respectively) in the extratropics.

To test our hypothesis that the observed differences between 2015/16 and 1997/98 were dominated by atmospheric noise, we first calculate the multimodel composite differences between the two events by averaging the two driest members for each model for 2015/16 and subtracting the average of the two wettest members for each model for 1997/98. Because the PNW and SOCAL indices are essentially uncorrelated, we define the driest and wettest members of by first constructing an index that is the difference between the PNW and SOCAL indices. Positive values of the index thus represent wetter conditions in the PNW and drier conditions in SOCAL, consistent with what was observed in 2015/16.

Negative values of the index reflect the opposite pattern, similar to what was observed in 1997/98. The multimodel composite thus represents the two members of each model with the strongest 2015/16-type anomaly minus the two members with the strongest 1997/98-type anomaly, averaged over all of the models in our study.

The full composite precipitation anomaly (Fig. 16a) is similar in both pattern and overall magnitude to the observed difference (cf. Fig. 14), demonstrating that the observed differences do lie within the range of possibilities the NMME is able to represent. Given that these are fully coupled seasonal forecast runs, we find this to be a somewhat remarkable achievement. Separating the composite into noise (deviation from ensemble mean) and ensemble-mean components (Figs. 16b and 16c, respectively) we find that the differences are dominated by the noise component, consistent with our analysis of the hindcast period. While there is a reduction in rainfall between 2015/16 and 1997/98 in the forced multimodel response (Fig. 13c), consistent with the forecast plumes in Fig. 3, the magnitude is low relative to the observed differences. The ensemble-mean anomaly also has its



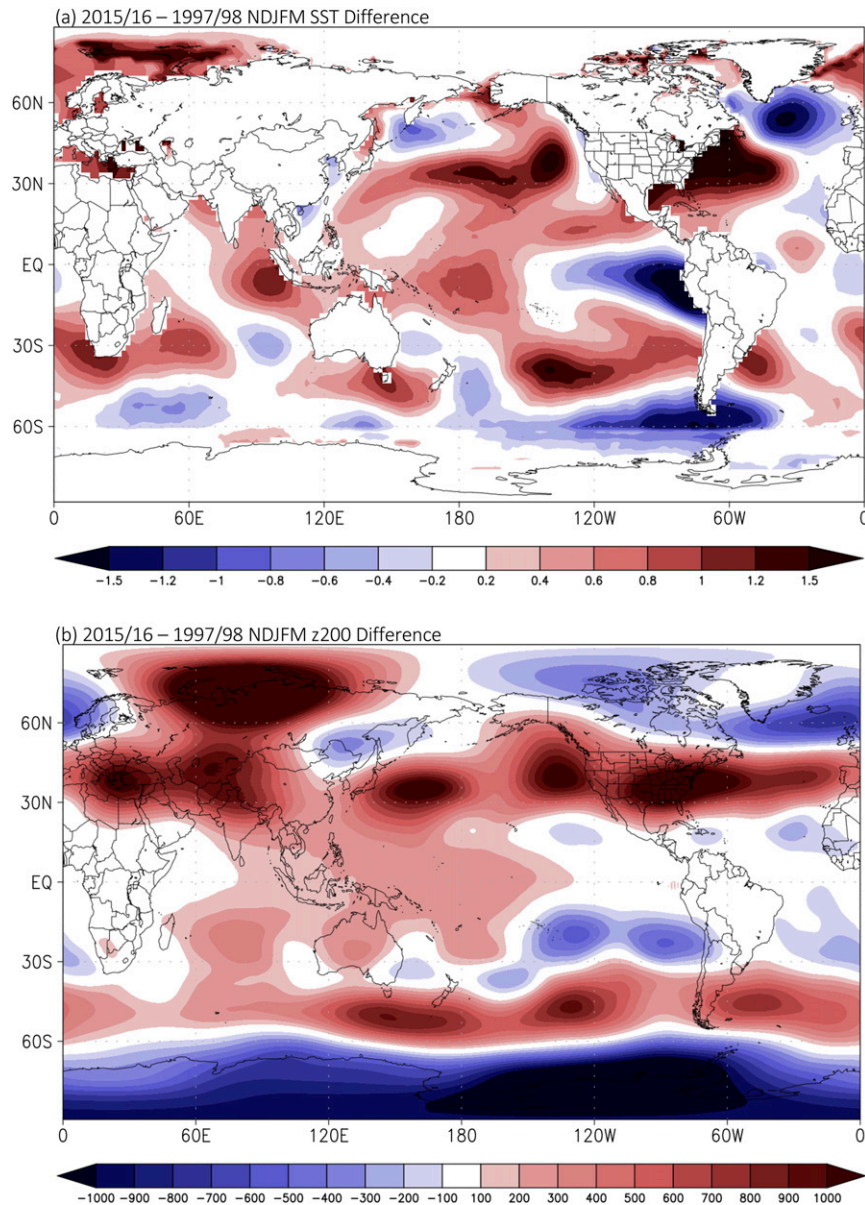


FIG. 15. Observed (a) SST (K) and (b) z200 (gpm) differences: NDJFM 2015/16 – 1997/98. Data from ERSSTv4 and ERA-Interim, respectively.

maximum in the node of the dipole, and thus contributes relatively little to anomaly in either region.

For the composite SST differences (Fig. 17a) the models again reproduce the observed differences to a reasonable degree (cf. to Fig. 15a). In contrast to the precipitation anomaly, however, the differences between 2015/16 and 1997/98 are dominated by the ensemble-mean component (Fig. 17c). The unpredicted SST elements (Fig. 17b) are relatively weak and confined to the North Pacific, again consistent with the analysis of the hindcast period (see Figs. 6a and 7a). We thus find that the

observed SST differences between the 1997/98 and 2015/16 events were reasonably well represented by the predicted components of the models. However, these differences led to relatively small differences in total rainfall (Fig. 16c).

Turning our attention to the 200-hPa height field (Fig. 18), the model composite again does a reasonable job of capturing the structure and magnitude of the observed anomalies (cf. Figs. 15b and 18a), with a clear maximum in the North Pacific, although the magnitudes are lower. Looking at the differences in



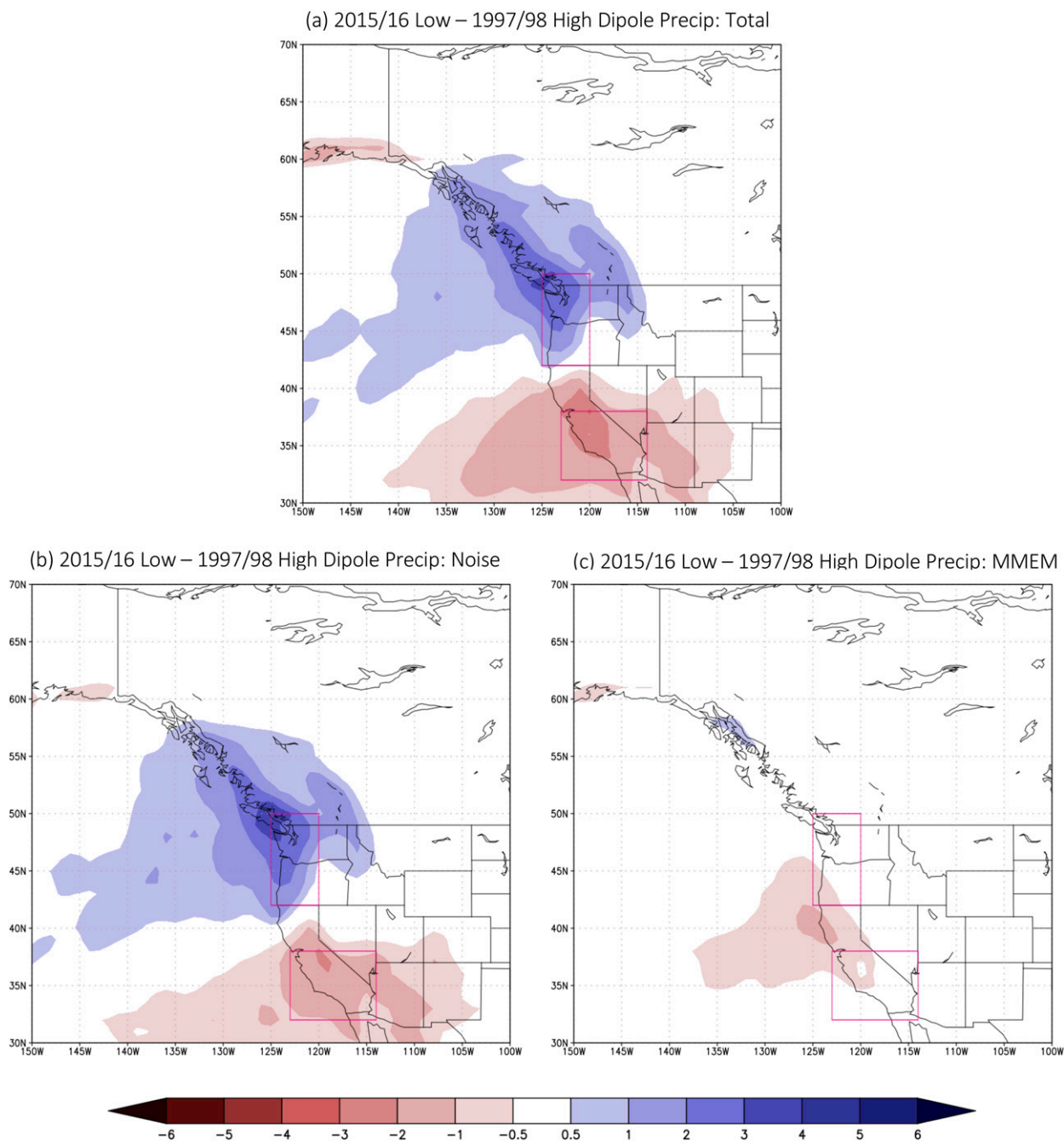


FIG. 16. Multimodel precipitation difference ( $\text{mm day}^{-1}$ ): (a) total, (b) noise, and (c) MMEM components. Driest NDJFM 2015/16 – wettest 1997/98 for dipole index.

the noise and ensemble-mean responses (Figs. 18b and 18c, respectively) it is interesting to note that the magnitudes of the two components are comparable in the North Pacific, with the noise component only slightly stronger. This is despite the fact that the noise component of precipitation composite is markedly stronger than the ensemble-mean component (see Figs. 16b,c),

suggesting that the rainfall response is quite sensitive to the exact location and orientation of the anomaly.

#### 4. Discussion

California experienced record levels of drought from 2012 to 2017. Despite the occurrence of a powerful

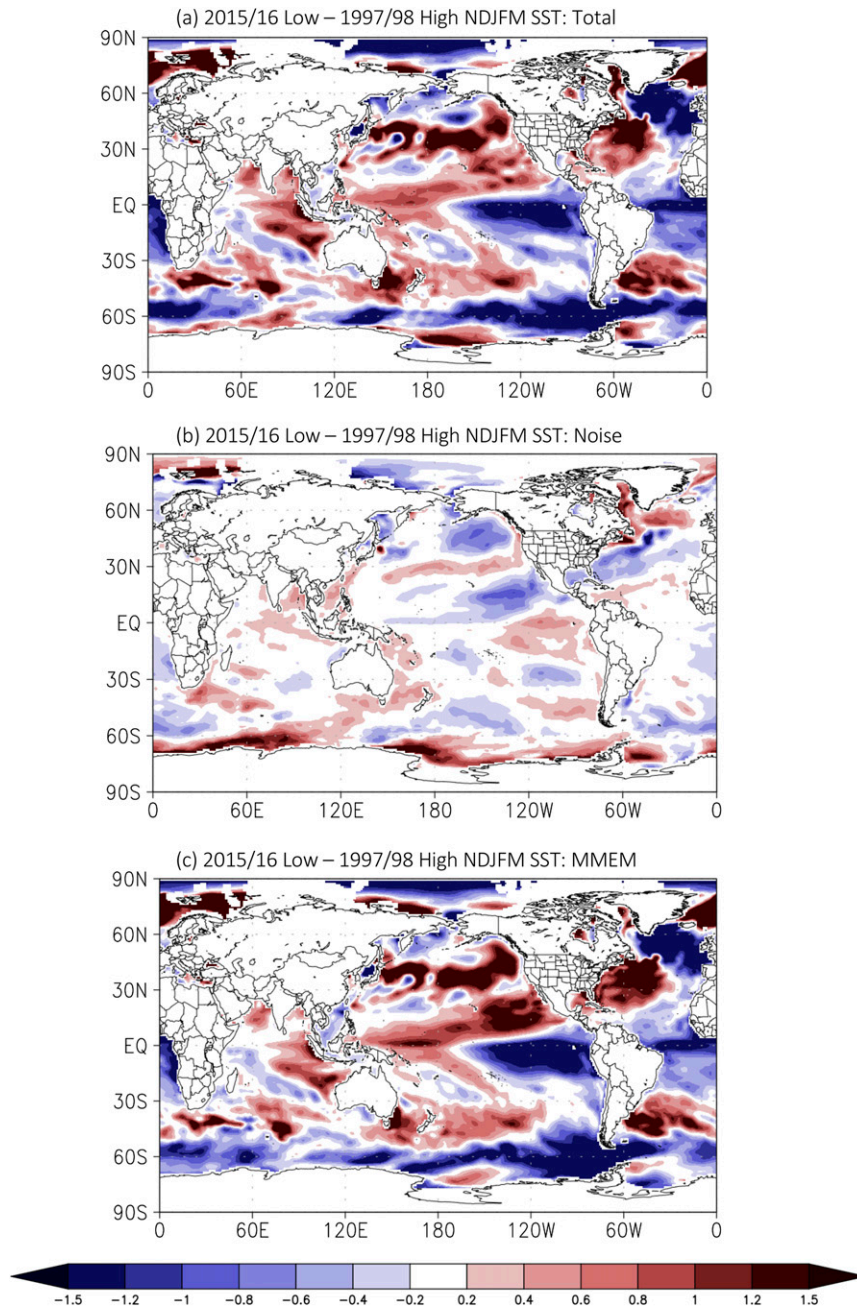


FIG. 17. Multimodel SST difference (K): (a) total, (b) noise, and (c) MMEM components. Driest NDJFM 2015/16 – wettest 1997/98 for dipole index.

El Niño event in 2015/16 Southern California experienced below-average and the Pacific Northwest above-average winter rainfall (Fig. 2c), confounding expectations based on both historical associations with ENSO and seasonal forecast models. In this work, we have examined the general relationship between winter rainfall along the West Coast of the United States and the El Niño–Southern Oscillation as well as the

2015/16 event in both models and observations. We find that while there is a statistically significant correlation between both PNW and SOCAL rainfall and Niño-3.4 for the recent historical period, Niño-3.4 explains at most one-third of the total rainy-season variance (see Fig. 1a). Thus, there is ample opportunity for other regions and fields to play a role in determining seasonal totals. Examination of previous large El Niño events

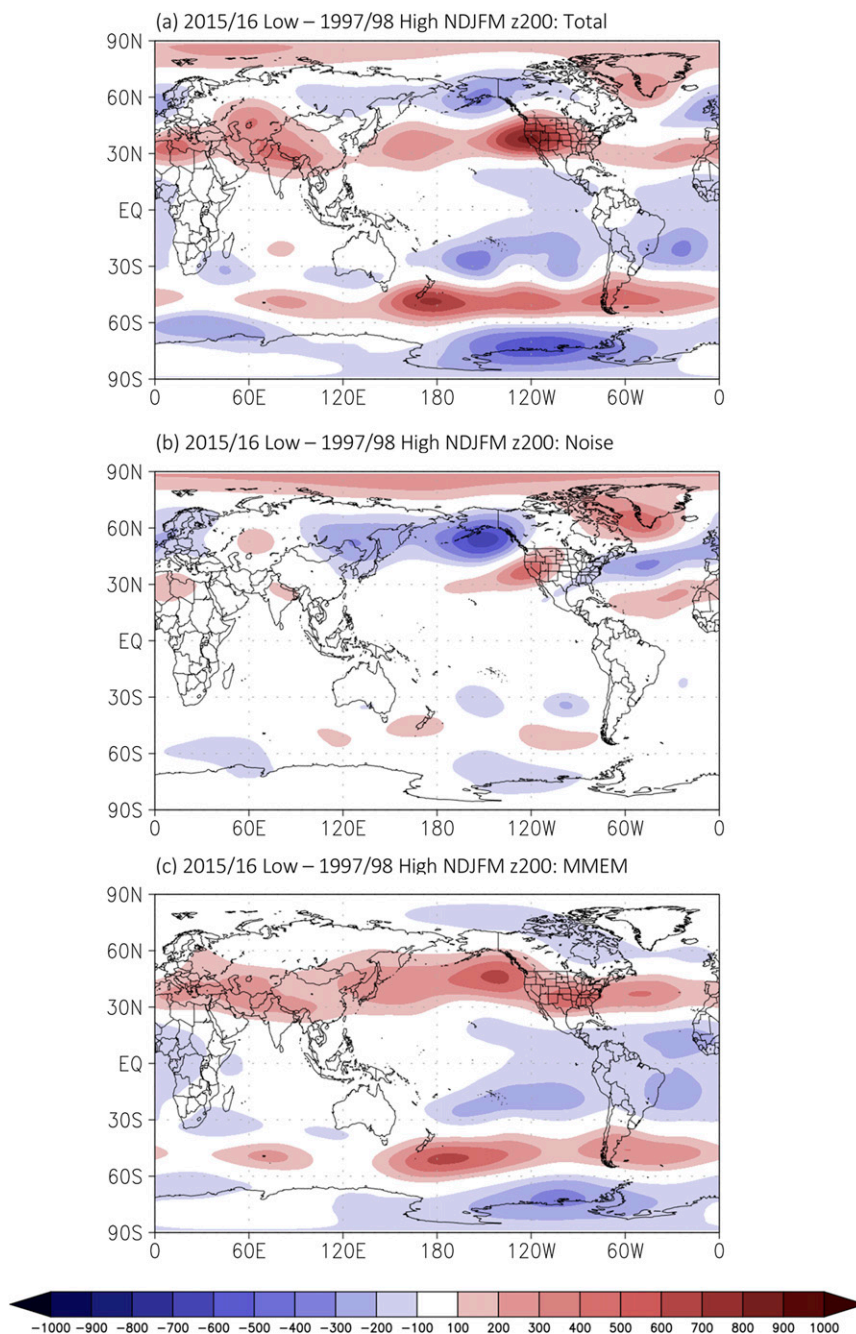


FIG. 18. Multimodel z200 difference (gpm): (a) total, (b) noise, and (c) MMEM components. Driest NDJFM 2015/16 – wettest 1997/98.

(1982/83, 1997/98; see Figs. 2a,b) also reveals significant variations in seasonal rainfall patterns and totals, further highlighting the importance of factors outside of the eastern tropical Pacific.

To identify these additional factors, we examine the large suite of individual model realizations available in the NMME archive. We find that the multimodel ensemble mean of the seasonal forecast runs, which emphasizes

the common elements of the forecast at the expense of the unpredictable elements, produces forecasts of above-average SOCAL rainfall for all three recent major events and below-average rainfall for the PNW in two out of the three (Fig. 3). The MMEM dramatically overstates the strength of the correlation between Niño-3.4 and rainfall in western North America (Fig. 4b). This result is consistent with those of



Wanders et al. (2017), who point out that the ensemble mean of the NMME models demonstrates a stronger sensitivity of precipitation to ENSO than the observations. However, we find that the models are capable of reproducing both the pattern and amplitude of the Niño-3.4–rainfall correlation with reasonable accuracy (Fig. 4a), subject to the somewhat counterintuitive requirement that the unpredictable elements are retained.

When the forecasts are separated into predictable and unpredictable components, the predictable component of SOCAL rainfall is strongly associated with tropical Pacific SST anomalies (Fig. 8b), as is the PNW (Fig. 7b). However, we find total rainfall in both regions is dominated by the noise component (Fig. 11b). The noise component of PNW shows a significant correlation with unpredicted SST in the Gulf of Alaska (Fig. 12a; the so-called Blob region), but SOCAL rainfall relatively little association with the noise component of SST (Fig. 12b). Ensemble members with increased (relative to the ensemble mean) SST in the Indian Ocean or central Pacific do not show consistent associations with unpredicted variations in SOCAL rainfall. Seasonal precipitation noise in both regions is instead strongly associated with unpredicted variations in 200-hPa height to the immediate northwest (Fig. 13), although it should be emphasized that this result is both model and field dependent, and application to a more predictable field like temperature or advances in modeling would be expected to produce a different partitioning.

The identification of the influence of predicted and unpredicted elements provides insights into the 2015/16 event and the differences in rainfall response to the “canonical” response in 1997/98. Consistent with previous studies we find that there are differences in the predicted component of rainfall between 2015/16 and 1997/98 (Fig. 16c), but that the predicted component accounts for a negligible amount of the observed differences. However, by including the noise component, the NMME can reproduce the observed differences across multiple fields. The primary driver of the differences between 2015/16 and 1997/98 in the NMME multimodel composite thus appears to have been unpredicted variations in the upper tropospheric circulation off the West Coast of the United States. Better understanding of the processes driving variability in this region could thus potentially lead to improved seasonal predictions of rainfall across the West Coast.

## 5. Conclusions

The 2015/16 El Niño event failed to bring increased winter-season precipitation to Southern California and

break the drought, despite predictions for above-average rainfall by multiple seasonal forecast models. This unexpected and unpredicted failure of the winter rains has prompted several recent studies (see the introduction), focusing on both the dynamical causes of the failed association with El Niño and the failure to predict it. Less emphasis has been given to the fact that forecasts also failed dramatically for the Pacific Northwest but in the opposite direction. Here we build on the findings of Wanders et al. (2017) by performing a rigorous evaluation of the predictable and unpredictable components of Pacific Northwest and California rainfall within the NMME and its association with predictable and unpredictable SST and dynamical forcings. Our analysis leads to the following central conclusions:

- 1) Although there is a statistically significant correlation between Niño-3.4 and both Southern California and Pacific Northwest rainfall, this relationship explains a relatively small fraction of the total rainfall variance even at its maximum. The fact that individual events deviate from this pattern is relatively unsurprising in this context.
- 2) When information from the individual ensemble members is retained, the NMME models correctly capture the correlation between West Coast rainfall and tropical Pacific SSTs (cf. Fig. 6 with Figs. 7a and 8a). However, they compare less favorably for the Indian and Atlantic basins, suggesting that the association between SST variability in these basins and SOCAL precipitation may be incorrectly represented in the models. The models also generally capture the relationship with 200-hPa heights (cf. Figs. 9 and 10).
- 3) The multimodel ensemble mean reduces the influence of unpredicted variability by design, thus drastically overestimates the strength of the relationship between California rainfall and tropical Pacific SSTs (Figs. 7b and 8b). This is consistent with the central finding of Wanders et al. (2017).
- 4) Southern California and Pacific Northwest rainfall variability is dominated by unpredicted variations (Fig. 11), and the unpredicted variations in rainfall are strongly correlated with unpredicted variations in the 200-hPa height field (Fig. 13). The correlation between unpredicted rainfall and unpredicted SST is relatively weak and confined to the extratropics (Fig. 12), although for the PNW there is an intriguing correlation with SST in the Gulf of Alaska (Fig. 12a) that suggests improving SST forecasts in this region could lead to improved seasonal forecasts in the NMME.
- 5) Composites of individual wet and dry ensemble members from 1997/98 and 2015/16 can encompass the



observed differences, with the greatest differences in precipitation and circulation arising from the unpredicted components. We thus conclude that unpredicted atmospheric variability was primarily responsible for the unexpectedly dry conditions in Southern California and wet conditions in the Pacific Northwest in the winter of 2015/16.

**Acknowledgments.** This research is supported by grants from the National Science Foundation (NSF) (AGS-1613318, AGS-1338427, AGS-1740693), the National Oceanic and Atmospheric Administration (NOAA) (NA14OAR4310160), and NASA (NNX14AM19G). Partial support for this work was provided by a firm fixed-price subcontract to George Mason University (18-GMU01) from Innovim LLC under prime contract DG133W-12-CQ-0008/TO016 from Climate Prediction Center, National Centers for Environmental Prediction. N.J.B. is supported by the Alfred P. Sloan Foundation as a Research Fellow.

## REFERENCES

- Cash, B. A., and Coauthors, 2017: Sampling variability and the ENSO–monsoon relationship. *Climate Dyn.*, **48**, 4071–4079, <https://doi.org/10.1007/s00382-016-3320-3>.
- Chen, M., W. Shi, P. Xie, V. B. S. Silva, V. E. Kousky, R. W. Higgins, and J. E. Janowiak, 2008: Assessing objective techniques for gauge-based analyses of global daily precipitation. *J. Geophys. Res.*, **113**, D04110, <https://doi.org/10.1029/2007JD009132>.
- Chen, X., and T. Zhou, 2014: Relative role of tropical SST forcing in the 1990s periodicity change of the Pacific–Japan pattern interannual variability. *J. Geophys. Res. Atmos.*, **119**, 13 043–13 066, <https://doi.org/10.1002/2014JD022064>.
- DelSole, T., and J. Shukla, 2012: Climate models product skillful predictions of Indian summer monsoon rainfall. *Geophys. Res. Lett.*, **39**, L09703, <https://doi.org/10.1029/2012GL051279>.
- Delworth, T. L., and Coauthors, 2006: GFDL’s CM2 global coupled climate models. Part I: Formulation and simulation characteristics. *J. Climate*, **19**, 643–674, <https://doi.org/10.1175/JCLI3629.1>.
- Dettinger, M. D., D. R. Cayan, H. F. Diaz, and D. M. Meko, 1998: North–south precipitation patterns in western North America on interannual-to-decadal timescales. *J. Climate*, **11**, 3095–3111, [https://doi.org/10.1175/1520-0442\(1998\)011<3095:NSPPIW>2.0.CO;2](https://doi.org/10.1175/1520-0442(1998)011<3095:NSPPIW>2.0.CO;2).
- , F. M. Ralph, T. Das, P. J. Neiman, and D. R. Cayan, 2011: Atmospheric rivers, floods and the water resources of California. *Water*, **3**, 445–478, <https://doi.org/10.3390/w3020445>.
- Gershunov, A., N. Schneider, and T. Barnett, 2001: Low-frequency modulation of the ENSO–Indian monsoon rainfall relationship: Signal or noise? *J. Climate*, **14**, 2486–2492, [https://doi.org/10.1175/1520-0442\(2001\)014<2486:LFMOT>2.0.CO;2](https://doi.org/10.1175/1520-0442(2001)014<2486:LFMOT>2.0.CO;2).
- Guan, B., and D. E. Waliser, 2015: Detection of atmospheric rivers: Evaluation and application of an algorithm for global studies. *J. Geophys. Res. Atmos.*, **120**, 12 514–12 535, <https://doi.org/10.1002/2015JD024257>.
- Hoell, A., M. Hoerling, J. K. Eischeid, K. Wolter, R. Dole, J. Perlwitz, T. Xu, and L. Cheng, 2016: Does El Niño intensity matter for California precipitation? *Geophys. Res. Lett.*, **43**, 819–825, <https://doi.org/10.1002/2015GL067102>.
- Hoerling, M. P., A. Kumar, and M. Zhong, 1997: El Niño, La Niña, and the nonlinearity of their teleconnections. *J. Climate*, **10**, 1769–1786, [https://doi.org/10.1175/1520-0442\(1997\)010<1769:ENOLNA>2.0.CO;2](https://doi.org/10.1175/1520-0442(1997)010<1769:ENOLNA>2.0.CO;2).
- Huang, B., and Coauthors, 2015a: Extended Reconstructed Sea Surface Temperature version 4 (ERSST.v4): Part I. Upgrades and intercomparisons. *J. Climate*, **28**, 911–930, <https://doi.org/10.1175/JCLI-D-14-00006.1>.
- , and Coauthors, 2015b: Extended Reconstructed Sea Surface Temperature (ERSST), version 4. 1980–2010. NOAA National Centers for Environmental Information, accessed December 2016, <https://doi.org/10.7289/V5KD1VVF>.
- Infanti, J. M., and B. P. Kirtman, 2016: North American rainfall and temperature prediction response to the diversity of ENSO. *Climate Dyn.*, **46**, 3007–3023, <https://doi.org/10.1007/s00382-015-2749-0>.
- Jong, B.-T., M. Ting, and R. Seager, 2016: El Niño’s impact on California precipitation: Seasonality, regionality, and El Niño intensity. *Environ. Res. Lett.*, **11**, 054021, <https://doi.org/10.1088/1748-9326/11/5/054021>.
- Kim, H.-M., Y. Zhou, and M. A. Alexander, 2017: Changes in atmospheric rivers and moisture transport over the Northeast Pacific and western North America in response to ENSO diversity. *Climate Dyn.*, <https://doi.org/10.1007/s00382-017-3598-9>.
- Kirtman, B. P., and D. Min, 2009: Multimodel ensemble ENSO prediction with CCSM and CFS. *Mon. Wea. Rev.*, **137**, 2908–2930, <https://doi.org/10.1175/2009MWR2672.1>.
- , and Coauthors, 2014: The North American Multimodel Ensemble: Phase-1 seasonal-to-interannual prediction; phase-2 toward developing intraseasonal prediction. *Bull. Amer. Meteor. Soc.*, **95**, 585–601, <https://doi.org/10.1175/BAMS-D-12-00050.1>.
- Kumar, K. K., B. Rajagopalan, and M. Cane, 1999: On the weakening relationship between the Indian monsoon and ENSO. *Science*, **284**, 2156–2159, <https://doi.org/10.1126/science.284.5423.2156>.
- Kwon, M., J. G. Jhun, B. Wang, S.-I. An, and J.-S. Kug, 2005: Decadal change in relationship between East Asian and WNP summer monsoons. *Geophys. Res. Lett.*, **32**, L16709, <http://doi.org/10.1029/2005GL023026>.
- Lee, S.-K., H. Lopez, E.-S. Chung, P. DiNezio, S.-W. Yeh, and A. T. Wittenberg, 2017: On the fragile relationship between El Niño and California rainfall. *Geophys. Res. Lett.*, **45**, 907–915, <https://doi.org/10.1002/2017GL076197>.
- Lim, Y.-K., S. D. Schubert, Y. Chang, A. M. Molod, and S. Pawson, 2018: The impact of SST-forced and unforced teleconnections on 2015/16 El Niño winter precipitation over the western United States. *J. Climate*, **31**, 5825–5844, <https://doi.org/10.1175/JCLI-D-17-0218.1>.
- McCabe, G. J., and M. D. Dettinger, 1999: Decadal variations in the strength of ENSO teleconnections with precipitation in the western United States. *Int. J. Climatol.*, **19**, 1399–1410, [https://doi.org/10.1002/\(SICI\)1097-0088\(19991115\)19:13<1399::AID-JOC457>3.0.CO;2-A](https://doi.org/10.1002/(SICI)1097-0088(19991115)19:13<1399::AID-JOC457>3.0.CO;2-A).
- Merryfield, W. J., and Coauthors, 2013: The Canadian Seasonal to Interannual Prediction System. Part I: Models and initialization. *Mon. Wea. Rev.*, **141**, 2910–2945, <https://doi.org/10.1175/MWR-D-12-00216.1>.

- Mo, K. C., and R. W. Higgins, 1998: Tropical influences on California precipitation. *Int. J. Climatol.*, **11**, 412–430, [https://doi.org/10.1175/1520-0442\(1998\)011<0412:TIOCP>2.0.CO;2](https://doi.org/10.1175/1520-0442(1998)011<0412:TIOCP>2.0.CO;2).
- Myoung, B., and Y. Deng, 2009: Interannual variability of the cyclone activity along the U.S. Pacific Coast: Influences on the characteristics of winter precipitation in the western United States. *J. Climate*, **22**, 5732–5747, <https://doi.org/10.1175/2009JCLI2889.1>.
- Quan, X.-W., M. Hoerling, L. Smith, J. Perlwitz, T. Zhang, A. Hoell, K. Wolter, and J. Eischeid, 2018: Extreme California rains during winter 2015/16: A change in El Niño teleconnection? *Bull. Amer. Meteor. Soc.*, **99**, S49–S53, <https://doi.org/10.1175/BAMS-D-17-0118.1>.
- Saha, S. K., and Coauthors, 2014: The NCEP Climate Forecast System version 2. *J. Climate*, **27**, 2185–2208, <https://doi.org/10.1175/JCLI-D-12-00823.1>.
- Schonher, T., and S. E. Nicholson, 1989: The relationship between California rainfall and ENSO events. *J. Climate*, **2**, 1258–1269, [https://doi.org/10.1175/1520-0442\(1989\)002<1258:TRBCRA>2.0.CO;2](https://doi.org/10.1175/1520-0442(1989)002<1258:TRBCRA>2.0.CO;2).
- Seager, R., N. Naik, M. Ting, M. A. Cane, N. Harnik, and Y. Kushnir, 2010: Adjustment of the atmospheric circulation to tropical Pacific SST anomalies: Variability of transient eddy propagation in the Pacific–North America sector. *Quart. J. Roy. Meteor. Soc.*, **136**, 277–296, <https://doi.org/10.1002/qj.588>.
- Siler, N., Y. Kosaka, S.-P. Xie, and X. Li, 2017: Tropical ocean contributions to California’s surprisingly dry El Niño of 2015/16. *J. Climate*, **30**, 10067–10079, <https://doi.org/10.1175/JCLI-D-17-0177.1>.
- Trenberth, K. E., G. W. Branstator, D. Karoly, A. Kumar, N.-C. Lau, and C. Ropelewski, 1998: Progress during TOGA in understanding and modeling global teleconnections associated with tropical sea surface temperatures. *J. Geophys. Res.*, **103**, 14 291–14 324, <https://doi.org/10.1029/97JC01444>.
- Vecchi, G. A., and Coauthors, 2014: On the seasonal forecasting of regional tropical cyclone activity. *J. Climate*, **27**, 7994–8016, <https://doi.org/10.1175/JCLI-D-14-00158.1>.
- Vernieres, G., M. M. Rienecker, R. Kovach, and C. L. Keppenne, 2012: The GEOS-iODAS, description and evaluation. NASA Technical Report Series on Global Modeling and Data Assimilation, NASA/TM-2012-104606, Vol. 30, 58 pp., <https://ntrs.nasa.gov/archive/nasa/casi.ntrs.nasa.gov/20140011278.pdf>.
- Wanders, N., and Coauthors, 2017: Forecasting the hydroclimatic signature of the 2015/16 El Niño event on the western United States. *J. Hydrometeorol.*, **18**, 177–186, <https://doi.org/10.1175/JHM-D-16-0230.1>.
- Xie, P., and P. A. Arkin, 1997: Global precipitation: A 17-year monthly analysis based on gauge observations, satellite estimates, and numerical model outputs. *Bull. Amer. Meteor. Soc.*, **78**, 2539–2558, [https://doi.org/10.1175/1520-0477\(1997\)078<2539:GPAYMA>2.0.CO;2](https://doi.org/10.1175/1520-0477(1997)078<2539:GPAYMA>2.0.CO;2).
- , A. Yatagai, M. Chen, T. Hayasaka, Y. Fukushima, C. Liu, and S. Yang, 2007: A gauge-based analysis of daily precipitation over East Asia. *J. Hydrometeorol.*, **8**, 607–626, <https://doi.org/10.1175/JHM583.1>.
- Yu, J.-Y., and Y. Zou, 2013: The enhanced drying effect of central-Pacific El Niño on US winter. *Environ. Res. Lett.*, **8**, 014019, <https://doi.org/10.1088/1748-9326/8/1/014019>.